

## Highlights

### **Efficacy of reduced order source terms for a coupled wave-circulation model in the Gulf of Mexico**

Mark Loveland, Jessica Meixner, Eirik Valseth, Clint Dawson

- ADCIRC+SWAN models Hurricane Ida and with various source term choices for SWAN
- Reduced order source terms (1st, 2nd gen) reduce run time by nearly half
- Source terms had larger impact on wave statistics than water surface elevations

# Efficacy of reduced order source terms for a coupled wave-circulation model in the Gulf of Mexico

Mark Loveland<sup>a,\*</sup>, Jessica Meixner<sup>b</sup>, Eirik Valseth<sup>a,c,d</sup> and Clint Dawson<sup>a</sup>

<sup>a</sup>Oden Institute for Computational Engineering and Sciences, University of Texas at Austin, Oden Institute for Computational Engineering and Sciences, The University of Texas at Austin, 201 E. 24th St., Austin, 78712, Texas, USA

<sup>b</sup>NWS/NCEP/Environmental Modeling Center, National Oceanic and Atmospheric Administration (NOAA), College Park, MD, USA

<sup>c</sup>The Department of Data Science, The Norwegian University of Life Science, Drøbakveien 31, Ås, 1433, Norway

<sup>d</sup>Department of Scientific Computing and Numerical Analysis, Simula Research Laboratory, Kristian Augusts gate 23, Oslo, 0164, Norway

---

## ARTICLE INFO

### Keywords:

Spectral wind wave model  
Shallow water equations  
Source terms  
ADCIRC  
SWAN

## ABSTRACT

During hurricanes, coupled wave-circulation models are critical tools for public safety. The standard approach is to use a high fidelity circulation model coupled with a wave model which uses the most advanced source terms. As a result, the models can be highly computationally expensive and so this study investigates the potential consequences of using highly simplified (reduced order) source terms within the wave model component of the coupled wave-circulation model. The trade-off between run time and accuracy with respect to observations is quantified for a set of two storms that impacted the Gulf of Mexico, Hurricane Ike and Hurricane Ida. Water surface elevations as well as wave statistics (significant wave height, peak period, and mean wave direction) are compared to observations. The usage of the reduced order source terms yielded significant savings in computational cost. Additionally, relatively low amounts of additional error with respect to observations during the simulations with reduced order source terms. However, large changes in global model outputs of the wave statistics were observed based on the choice of source terms particularly near the track of each hurricane.

---

## 1. Introduction

During tropical cyclones, the destructive impacts of wind waves and storm surge can be hazardous for local populations, infrastructure, flora, and fauna. Accurate numerical models are important tools in preparation for such events so that forecasts can be made and emergency measures may be taken to avoid unnecessary damage. It has been shown that the interaction between wind waves and the surge plays a significant role in the overall storm surge levels via wave-induced set up and wave-induced set down [39]. This observed interaction has resulted in the development of coupled spectral wave and circulation models, which model both wind waves and storm surge respectively, to improve model accuracy. In this study we will focus on coupled models that use a spectral wave model governed by the Wave Action Balance Equation (WAE), and a circulation model governed by the Shallow Water Equations. There are many operational-scale models of this kind that include coupling between circulation and wind waves to predict storm surge and wave statistics including ADCIRC+SWAN [10], ADCIRC+STWAVE [8, 11], AdH+STWAVE [41], ADCIRC+WAVEWATCHIII [44], and SCHISM-WWMIII [52]. Spectral wave models are expensive and in particular the computation of the source terms within the models can take a large portion of the computing load. The inclusion of the spectral wave model increases total run times by as much as triple that of a standalone circulation model. [50, 42, 34, 1, 45, 30, 32, 52].

The source terms within the context of the WAE are both complex and highly empirical due to the complex nature of the physics it is trying to approximate and is still an active area of research [34, 1]. Since the latter half of the 20th century, the general format of the source terms for the WAE has remained relatively unchanged, and is often written as a sum of wind input ( $S_{in}$ ), nonlinear interaction ( $S_{nl}$ ), and dissipation ( $S_{diss}$ ), though the specific parameterizations of these are always evolving [32]. The choice of source terms can strongly influence not only the accuracy of results but can also strongly influence computational cost [34, 1, 53]. In this study we seek to quantify the trade-off between the accuracy and the computational cost due to source term choices, specifically in the coupled wave-circulation setting.

---

\*Corresponding author

 [markloveland@utexas.edu](mailto:markloveland@utexas.edu) (M. Loveland)

 <https://www.researchgate.net/profile/Mark-Loveland-2> (M. Loveland)

ORCID(s): 0000-0002-2164-2884 (M. Loveland); 0000-0001-6940-4191 (E. Valseth); 0000-0001-7273-0684 (C. Dawson)

Operational wave-circulation models often utilize the latest, most accurate source terms available for the given wave model [10, 8, 41, 44, 52]. These source term packages are referred to as 3rd generation source terms because they explicitly approximate the full nonlinear interactions contained in the aforementioned  $S_{nl}$  term [53, 34]. The two main physical processes that  $S_{nl}$  accounts for are called three-wave interactions (triads) and four-wave interactions (quadruplets) [34, 30, 28]. These processes are both known to be highly computationally expensive to approximate accurately and therefore even the most cutting edge 3rd generation source term packages rely on very crude approximations [1]. The most common methods to approximate the triads and quadruplets are the lumped triad approximation (LTA) [15] and discrete interaction approximation (DIA) [25] respectively. Even these rough approximations can still be computationally expensive, and so part of this study is to see how much cost can be saved and what accuracy is sacrificed if these processes are either neglected or highly simplified within the coupled wave-circulation setting.

It is also noted that there is still an ongoing debate on the physical accuracy namely of the source term packages relying on the DIA [2]. This has motivated work on finding parametric relations for waves generated by hurricanes to reduce model cost while still incorporating effects from waves [64]. Furthermore, there has been investigation into using reduced order or parametric models for the spectral waves to force circulation models [7]. This work seeks to look further into this direction by looking into the usage of 1st and 2nd generation source terms for the wave model within the coupled wave-circulation setting. 1st and 2nd generation source terms are characterized by either negligence or severe simplification of the nonlinear source term  $S_{nl}$  [53]. For a more detailed exposition into the specifics of the distinction between 1st, 2nd, and 3rd generation of source terms we refer to Appendix A.

In this study, ADCIRC+SWAN, will be used to investigate the trade-off between computational performance and accuracy of 1st, 2nd, and 3rd generation source term parameterizations within SWAN. In particular, this work will focus on the impacts of utilizing the reduced-order physics of the 1st and 2nd generation source term choices within ADCIRC+SWAN when compared to the more commonly used 3rd generation source terms. The accuracy of the models will be quantified by looking at both SWAN wave statistic output compared to real buoys as well as ADCIRC water surface elevation (WSE) output compared to real gauges. The computational performance of the models will be quantified by tabulating wall clock times.

Following this introductory section, in Section 2, ADCIRC+SWAN will briefly be described along with the source term packages used within SWAN. Next, in Section 3 the specific storms used in this study, Hurricanes Ike and Ida, will be discussed and presented in detail. Then in Section 4, the specific configuration for each ADCIRC+SWAN will be outlined in detail. The results of all of the simulations are shown and analyzed against field data in Section 5. Finally, conclusions and comments on potential future directions of work are drawn in Section 6.

## 2. Model Details

### 2.1. The ADCIRC+SWAN Model

The shallow water model that is coupled to SWAN is called the Advanced Circulation Model (ADCIRC) [40]. ADCIRC is a finite element model that solves the shallow water equations (SWE) on unstructured triangular meshes and is used often to predict tides and storm surges [61]. Both standalone ADCIRC and the coupled model ADCIRC+SWAN have been validated in many realistic scenarios such as Hurricane Katrina, Hurricane Rita, Hurricane Ike, and is currently used operationally for forecasting and hindcasting [10, 12, 17, 29].

The coupled model (ADCIRC+SWAN) works through a tight, sequential coupling set up where ADCIRC is run for some time and the resulting WSE and mean water velocities are passed as inputs to SWAN. SWAN then runs given this information and then outputs wave radiation stress, which is added as forcing into the momentum equations of ADCIRC [10]. Both ADCIRC and SWAN are run on the same unstructured mesh, which eliminates the need for interpolation of WSE, water velocities, wave radiation stresses, bathymetry, or wind inputs.

ADCIRC obtains the WSE by solving the Generalized Wave Continuity Equation (GWCE) version of the SWE, which is obtained by differentiation of the continuity equation of the SWE in time and addition of the momentum

equations of the SWE [40]. ADCIRC subsequently solves the weak form of the GWCE using the standard Bubnov-Galerkin method using linear polynomial basis functions and is reproduced below. Find  $\zeta_i \in U_h(\Omega)$ :

$$\begin{aligned} & \left( \frac{\partial^2 \zeta_i}{\partial t^2}, \phi_j \right)_\Omega + \left( \tau_o \frac{\partial \zeta_i}{\partial t}, \phi_j \right)_\Omega + (gh_i \nabla \zeta_i, \nabla \phi_j)_\Omega = \\ & \left( \mathbf{J}_i, \nabla \phi_j \right)_\Omega + \left( Q_x \frac{\partial \tau_o}{\partial x}, \phi_j \right)_\Omega + \left( Q_y \frac{\partial \tau_o}{\partial y}, \phi_j \right)_\Omega - \left( \frac{\partial \mathbf{Q}}{\partial t} \cdot \mathbf{n} + \tau_o \mathbf{Q} \cdot \mathbf{n}, \phi_j \right)_\Gamma \quad \forall \phi_j \in V_h(\Omega). \end{aligned} \quad (1)$$

In this case,  $\zeta_i$ , is the WSE relative to a geoid,  $\tau_o$  is a tunable function for numerical stability,  $\mathbf{n}$  is the outward pointing normal vector on the domain boundary  $\Gamma$ ,  $h_i$  is the bathymetric depth to the bottom,  $\mathbf{J}_i$  is a vector quantity representing momentum flux and is defined as:

$$\mathbf{J} = \begin{Bmatrix} J_x \\ J_y \end{Bmatrix} = \begin{Bmatrix} -Q_x \frac{\partial U}{\partial x} - Q_y \frac{\partial U}{\partial y} + f Q_y - \frac{g}{2} \frac{\partial \zeta^2}{\partial x^2} - gd \frac{\partial}{\partial x} \left[ \frac{P_s}{g\rho} - \alpha\gamma \right] \\ + \frac{\tau_{sx,wind} + \tau_{sx,waves} - \tau_{bx}}{\rho} + M_x - D_x + U \frac{\partial \zeta}{\partial t} + \tau_o Q_x - gd \frac{\partial \zeta}{\partial x} \\ -Q_x \frac{\partial V}{\partial x} - Q_y \frac{\partial V}{\partial y} + f Q_x - \frac{g}{2} \frac{\partial \zeta^2}{\partial y^2} - gd \frac{\partial}{\partial y} \left[ \frac{P_s}{g\rho} - \alpha\gamma \right] \\ + \frac{\tau_{sy,wind} + \tau_{sy,waves} - \tau_{by}}{\rho} + M_y - D_y + V \frac{\partial \zeta}{\partial t} + \tau_o Q_y - gd \frac{\partial \zeta}{\partial y} \end{Bmatrix}. \quad (2)$$

In the above equation we have the depth-averaged velocities in the x and y direction as  $U, V$  respectively; the vector  $\mathbf{Q} = (Q_x, Q_y)$  represents momentum and is equal  $(Ud, Vd)$ ;  $d = \zeta + h$  is the total water depth;  $f$  is the Coriolis force parameter;  $g$  is the constant of gravitational acceleration;  $P_s$  is the atmospheric pressure at the surface;  $\rho$  is the density of water;  $\alpha$  is the effective earth elasticity factor;  $\gamma$  is the tidal potential factor;  $\tau_{sx,wind}, \tau_{sy,wind}$  are the wind stresses in the x and y direction;  $\tau_{sx,waves}, \tau_{sy,waves}$  are the stresses in the x and y directions from wind waves, which we discuss later;  $\tau_{bx}, \tau_{by}$  are the bottom stresses in both x and y;  $M_x, M_y$  represent the lateral stress gradient;  $D_x, D_y$  represent momentum dispersion. In addition to the GWCE, ADCIRC also solves the weak form of the two momentum conservation equations from the shallow water equations in non-conservative form to form a complete system of equations as in [40]. From (1), the ADCIRC model produces an approximate water depth,  $d$ , and depth-averaged velocities  $U, V$  that are used as inputs into the SWAN model. Then the SWAN model produces an approximation to the WAE and outputs wave radiation stresses used to compute the aforementioned wave stresses,  $\tau_{sx,waves}, \tau_{sy,waves}$ . The wave stresses are estimated as:

$$\begin{aligned} \tau_{sx,waves} &= -\frac{\partial S_{xx}}{\partial x} - \frac{\partial S_{xy}}{\partial y}, \\ \tau_{sy,waves} &= -\frac{\partial S_{xy}}{\partial x} - \frac{\partial S_{yy}}{\partial y}, \end{aligned} \quad (3)$$

where  $S_{xx}, S_{xy}, S_{yy}$  are the wave radiation stresses computed with SWAN output and defined as:

$$\begin{aligned} S_{xx} &= \rho g \int_{-\pi}^{\pi} \int_{\sigma_{min}}^{\sigma_{max}} (n \cos^2(\theta) + n - \frac{1}{2}) \sigma N d\sigma d\theta, \\ S_{xy} &= \rho g \int_{-\pi}^{\pi} \int_{\sigma_{min}}^{\sigma_{max}} n \sin(\theta) \cos(\theta) \sigma N d\sigma d\theta, \\ S_{yy} &= \rho g \int_{-\pi}^{\pi} \int_{\sigma_{min}}^{\sigma_{max}} (n \sin^2(\theta) + n - \frac{1}{2}) \sigma N d\sigma d\theta, \end{aligned} \quad (4)$$

where  $N$  is the action balance,  $\sigma, \theta$  represents relative radial frequency and direction of the wave spectrum respectively. The variable  $n$  is related to propagation velocity and is defined as:

$$n = \frac{1}{2} \left( 1 + \frac{2kd}{\sinh(2kd)} \right), \quad (5)$$

where  $k$  is the wavenumber magnitude defined through the dispersion relation (8).

The SWAN model is defined through the wave action balance equation, the WAE is a linear, scalar-valued, hyperbolic equation in 4 dimensions with a varying (both in 4-D space and time), non-divergence free velocity field,  $(\mathbf{c}(x, y, \sigma, \theta))$ , which can be determined independently of the unknown  $N(x, y, \sigma, \theta)$ . This is different than most conservation laws such as Navier-Stokes and related transport equations because typically the propagation velocity is just a function of the unknown i.e.  $\mathbf{c}(N)$ .

The proper boundary and initial conditions are as follows, assuming we have a bounded domain in four-dimensional space  $\Omega \subset \mathbb{R}^4$  that is sufficiently regular. Similar to other advection problems, the boundary is split up into 2 segments, inflow and outflow:

$$\begin{aligned} \Gamma_- &= x \in \partial\Omega : \mathbf{c} \cdot \mathbf{n} < 0 = \text{inflow} \\ \Gamma_+ &= x \in \partial\Omega : \mathbf{c} \cdot \mathbf{n} \geq 0 = \text{outflow}, \end{aligned} \quad (6)$$

where  $\mathbf{n}$  is the outwards unit normal vector to the boundary. Then it has been shown that the following problem possesses a unique solution [38, 13, 47]:

$$\begin{aligned} N_t + \nabla \cdot (\mathbf{c}N) &= \frac{S(N, x, y, \sigma, \theta, t)}{\sigma} \quad \text{on } \Omega \times (0, T), \\ N &= N_- \quad \text{on } \Gamma_-, \\ N &= N_0 \quad \text{on } \Omega \quad \text{at } t = 0, \end{aligned} \quad (7)$$

where  $N_t$  denotes the (partial) time derivative of  $N$ ,  $S$  the source/sink terms,  $\Omega$  the computational domain, and  $N_-$  the specified essential boundary condition on the outflow boundary. In the case when  $S$  is either 0 or is independent of  $N$ , a fairly straightforward analytic solution to the above problem can be obtained via the method of characteristics [13]. However, in practice  $S$  is quite complex, often nonlinear, and realistic problems become too complex to analyze with pencil and paper and thus the need for numerical methods to approximately solve (7) arises.

The propagation velocities,  $\mathbf{c}$ , are all determined using the constitutive relation called the dispersion relation that is derived under assumptions of Airy Wave Theory. The dispersion relation relates relative radial frequency,  $\sigma$ , to wavenumber magnitude,  $k$ :

$$\sigma^2 = gk \tanh(kd). \quad (8)$$

Here  $g$  is the constant of gravitational acceleration and  $d$  is total water depth. The velocity  $\mathbf{c}$  is a non-constant, non-divergence free vector quantity defined as:

$$\mathbf{c} = (c_g \cos\theta + U, c_g \sin\theta + V, c_\sigma, c_\theta), \quad (9)$$

where  $U, V$  are the depth-averaged water velocities in  $x, y$  directions respectively (these come from ADCIRC),  $c_g$  the relative group velocity (defined as  $\frac{\partial\sigma}{\partial k}$ , whereas the absolute group velocity is  $\frac{\partial\omega}{\partial k} = c_g + \|(U, V)\|$ ), and  $c_\sigma, c_\theta$  define the advection of the spectra with respect to direction and relative frequency, respectively. The group velocity,  $c_g$ , can be directly obtained by differentiating the dispersion relation in (8) for relative frequency,  $\sigma$ , with respect to wavenumber magnitude  $k$ . The explicit expression is:

$$c_g = n \sqrt{\frac{g}{k} \tanh(kd)}, \quad (10)$$

where  $n$  is from (5). The propagation velocity  $c_\sigma$ , represents frequency shifting due to changes in depths and currents. By applying the chain rule, we can find an expression of  $c_\sigma$ :

$$\begin{aligned} c_\sigma &= \frac{d\sigma}{dt} = \frac{k\sigma}{\sinh(2kd)} \left( \frac{\partial d}{\partial t} + U \frac{\partial d}{\partial x} + V \frac{\partial d}{\partial y} \right) - \\ & c_g k \left( \frac{\partial U}{\partial x} \cos^2(\theta) + \frac{\partial U}{\partial y} \cos(\theta) \sin(\theta) + \frac{\partial V}{\partial x} \sin(\theta) \cos(\theta) + \frac{\partial V}{\partial y} \cos^2(\theta) \right). \end{aligned} \quad (11)$$

The complete derivation is quite lengthy and we refer interested readers to Appendix D in the text of Holthuijsen [28]. Now the propagation velocity  $c_\theta$ , with respect to  $\theta$ , represents the shift in the spectrum due to refraction and diffraction.

Similarly to  $c_\sigma$ , the derivation is quite lengthy but can be obtained by applying the chain rule:

$$c_\theta = \frac{d\theta}{dt} = \frac{\sigma}{\sinh(2kd)} \left( \frac{\partial d}{\partial x} \sin(\theta) - \frac{\partial d}{\partial y} \cos(\theta) \right) + \frac{\partial U}{\partial x} \cos(\theta) \sin(\theta) - \frac{\partial U}{\partial y} \cos^2(\theta) + \frac{\partial V}{\partial x} \sin^2(\theta) - \frac{\partial V}{\partial y} \cos(\theta) \sin(\theta). \quad (12)$$

## 2.2. SWAN Source Term Packages

In the definition of the Wave Action Balance Equation (7), the source term  $S(x, y, \sigma, \theta, t)$  was arbitrary. In practice, the source term  $S$  can take many forms but in general it can be thought of as a sum of three key sources/sinks:

$$S = S_{in} + S_{diss} + S_{nl}, \quad (13)$$

where  $S_{in}$  represents any contribution to the spectrum due to wind input and typically takes the form as a sum of linear and exponential wave growth:

$$S_{in} = \alpha + \beta E(x, y, \sigma, \theta, t), \quad (14)$$

where  $\alpha, \beta$  are parameters that will be discussed later.  $S_{diss}$  represents any change in the energy spectrum due to dissipation that can include things like whitecapping and surf zone breaking. For the purposes of this dissertation, only the most commonly used dissipation source terms will be included and are whitecapping, bottom friction, and depth-induced breaking:

$$S_{diss} = S_{wc} + S_{bf} + S_{br}. \quad (15)$$

$S_{nl}$  represents changes in the spectrum due to nonlinear wave interactions. In the following subsections we summarize the forms of the source term in the 3rd generation ST6 package as well as 1st and 2nd generation source terms that are implemented in SWAN and will be used in this study. A more general discussion of some of the available source terms in SWAN can be found in Appendix A. The ST6 package was chosen to represent the 3rd generation source terms because this is the latest available in the ADCIRC+SWAN software, and the specific implementations of the 1st and 2nd generation source term packages were chosen because they were the only ones readily available within the SWAN source code.

### 2.2.1. Full Source Terms (ST6)

In the last decade or so beginning with the work of Ardhuin, Babanin and many others [3], the latest third generation source term package has changed to become semi-empirical in an aim to agree better with observed data and specifically to be more robust to situations with extreme weather. This work culminated into new source terms for  $S_{in}$  and  $S_{wc}$ , and is often referred to as ST6, which was first fully defined in a paper by Rogers *et al.* in 2012 [49]. This source term package is available and widely used in both SWAN and WAVEWATCH III and will be used in this study. The wind input term for the ST6 package is defined as follows,  $\alpha = 0$  and  $\beta$  from (14) is given by:

$$\beta = \gamma \sigma \frac{\rho_{air}}{\rho_{water}}, \quad (16)$$

where  $\gamma$  is a parameter that depends on location, direction, and frequency as:

$$\gamma(x, y, f, \theta) = G(x, y, f, \theta) \sqrt{B_n(x, y, f)} W(x, y, f, \theta). \quad (17)$$

In this context  $f = \frac{\sigma}{2\pi}$  and  $G, B_n$ , and  $W$  are defined as:

$$G(x, y, f, \theta) = 2.8 - (1 + \tanh(10\sqrt{B_n(x, y, f)} W(x, y, f, \theta) - 11)), \quad (18)$$

$$B_n(x, y, f) = \frac{A(x, y, f)}{2\pi} E(x, y, f) k^3 c_g, \quad (19)$$

$$W(x, y, f, \theta) = (\max(0, \frac{U_{10}}{c} \cos(\theta - \theta_{wind}) - 1))^2. \quad (20)$$

Here,  $E(x, y, f)$  is the integrated spectrum  $E(x, y, f) = \int_{\theta} E(x, y, f, \theta) d\theta$ , where  $E(x, y, f, \theta) = E(x, y, \sigma, \theta) 2\pi$ .  $U_{10}$  is the wind speed at 10 m above the surface,  $\theta_{wind}$  is the direction of the wind, and  $c$  is wave celerity that is related by group velocity as defined in (10) through the relation:

$$c_g = nc, \quad (21)$$

where  $n$  is from (5).  $A(x, y, f)$  is the wave steepness defined by:

$$\frac{1}{A(x, y, f)} = \int_{\theta} E_n(x, y, f, \theta) d\theta, \quad (22)$$

where  $E_n(x, y, f, \theta)$  is  $\frac{E(x, y, f, \theta)}{E'(x, y, f)}$  and  $E'(x, y, f)$  is:

$$E'(x, y, f) = \max_{\theta} (E(x, y, f, \theta)). \quad (23)$$

For the ST6 source term package, the whitecapping term is defined in the following way:

$$S_{wc}(x, y, f, \theta) = \begin{cases} 0, & \text{if } E(x, y, f, \theta) < E_T(x, y, f, \theta) \\ T_1(x, y, f, \theta) + T_2(x, y, f, \theta) & \text{if } E(x, y, f, \theta) \geq E_T(x, y, f, \theta), \end{cases} \quad (24)$$

Where the threshold spectral density,  $E_T$ , is defined as:

$$E_T(x, y, f, \theta) = \frac{2\pi B_{nt}}{A(x, y, f) c_g k^3}, \quad (25)$$

with  $B_{nt}$  is a constant that by default is 1.225e-3 and  $A(x, y, f)$  as in (22). The two contributions of whitecapping are defined as follows:

$$\begin{aligned} T_1(x, y, f, \theta) &= a_1 A(x, y, f) f \left[ \frac{\Delta(x, y, f)}{E(x, y, f)} \right]^L E(x, y, f, \theta), \\ T_2(x, y, f, \theta) &= a_2 \left[ \int_{f_{low}}^f \left[ \frac{\Delta(x, y, f')}{E(x, y, f')} \right]^M df' \right] E(x, y, f, \theta). \end{aligned} \quad (26)$$

Constants  $a_1, a_2, L, M$  are calibrated based on empirical data and the function  $\Delta = E - E_T$  is the difference between variance density,  $E$ , and threshold variance density,  $E_T$ . In addition to the whitecapping and wind input prescribed by the ST6 formulation, bottom friction, depth-induced breaking, three-wave interactions and four-wave interactions are also included in the SWAN runs when 3rd generation sources are activated and the specific forms of the terms can be found in Appendix A. The default options in SWAN for bottom friction, and depth-induced breaking are used [54]. For nonlinear source terms, the Lumped Triad Approximation (LTA) is used for the three-wave interactions while the DIA is used for the four-wave interactions.

### 2.2.2. Reduced Order Source Terms

In addition to the ST6 source term package, which represents a 3rd generation type, SWAN contains a 1st generation and a 2nd generation source package as formulated in a study from Holthuijsen et. al. [27]. The 1st and 2nd generation source packages in SWAN, as defined in the technical manual, are reproduced here [54]:

$$S = \begin{cases} A + BE & E < E_{lim} & \& |\theta - \theta_{wind}| < \frac{\pi}{2} \\ \frac{E_{lim} - E}{\tau} & E > E_{lim} & \& |\theta - \theta_{wind}| < \frac{\pi}{2} \\ 0 & E > E_{lim} & \& |\theta - \theta_{wind}| \geq \frac{\pi}{2}. \end{cases} \quad (27)$$

The difference between the source term package of 1st and 2nd generation is the definition of the saturated spectrum  $E_{lim}$ . In (27),  $\theta_{wind}$  is the direction of incoming winds, and  $\tau$  is a time scale set to:

$$\tau = \beta_4 \left( \frac{2\pi}{\sigma} \right)^2 \frac{g}{U_{10} \cos(\theta - \theta_{wind})}, \quad (28)$$

with  $\beta_4 = 250$ . The linear growth term,  $A$ , is defined as:

$$A = \begin{cases} \frac{\beta_l \pi C_{drag}^2 \rho_{air}^2 (U_{10} \max[0, \cos(\theta - \theta_{wind}))]^4}{2\pi g^2 \rho_{water}^2} & \sigma \geq 0.7\sigma_{PM,d} \\ 0 & \sigma < \sigma_{PM,d}. \end{cases} \quad (29)$$

$\beta_l$  is a proportionality constant that is empirically tuned with default set to 188 and the drag coefficient is set to  $C_{drag} = 0.0012$ . The variable  $\sigma_{PM,d}$  represents the peak relative radian frequency of a Pierson-Moskowitz corrected for variable depths:

$$\sigma_{PM,d} = \frac{\sigma_{PM}}{\tanh(0.833\bar{d}^{-0.375})}. \quad (30)$$

The variable  $\bar{d}$  is dimensionless depth set to  $gd/(U_{10})^2$  and the Pierson-Moskowitz peak frequency  $\sigma_{PM} = 0.13g2\pi/U_{10}$ . The exponential growth term,  $B$ , in (27) is defined as:

$$B = \max[0, \beta_2 \frac{5\rho_{air}}{2\pi\rho_{water}} \left( \frac{U_{10} k \cos(\theta - \theta_{wind})}{\sigma} - \beta_3 \right) \sigma], \quad (31)$$

where the empirical constants are by default set to  $\beta_2 = 0.59$ ,  $\beta_3 = 0.12$ . The saturated spectrum,  $E_{lim}$ , is a modification of the Pierson-Moskowitz spectrum and is defined as:

$$E_{lim} = \begin{cases} \frac{\alpha k^{-3}}{2c_g} e^{-\frac{5}{4} \left( \frac{\sigma}{\sigma_{PM,d}} \right)^4} \frac{2}{\pi} \cos^2(\theta - \theta_{wind}) & |\theta - \theta_{wind}| < \frac{\pi}{2} \\ 0 & |\theta - \theta_{wind}| \geq \frac{\pi}{2}. \end{cases} \quad (32)$$

The parameter  $\alpha$  is what differentiates 1st generation from 2nd generation source packages. In the case of the 1st generation,  $\alpha = 0.0081$ .  $\alpha$  in the 2nd generation setting it is:

$$\alpha = \max[0.0081 + (0.013 - 0.0081)e^{-\bar{d}}, 0.0023 \tilde{E}_{tot,sea}^{-0.223}]. \quad (33)$$

$\tilde{E}_{tot,sea}$  is the total dimensionless wind sea wave energy defined as  $\tilde{E}_{tot,sea} = g^2 E_{tot,sea} / U_{10}^4$  with  $E_{tot,sea}$  defined as:

$$E_{tot,sea} = \int_{\theta_{wind} - \frac{\pi}{2}}^{\theta_{wind} + \frac{\pi}{2}} \int_{0.7\sigma_{PM,d}}^{\sigma_{max}} E d\sigma d\theta. \quad (34)$$

Now that we have established how exactly ADCIRC and SWAN influence one another as well as the source term configurations that will be used, we will describe the specific test cases used in this study.

### 3. Scenario Descriptions

#### 3.1. Hurricane Ike

Hurricane Ike is selected as a test case because there is plenty of data available for comparisons and because this specific scenario has already been validated with ADCIRC+SWAN in [29]. Hurricane Ike made landfall on September 13th, 2008 near the City of Galveston, Texas. Hurricane Ike was a category 4 hurricane with maximum sustained winds of 110 mph at the time of landfall in Galveston [9]. Hurricane Ike produced billions of dollars in damages and induced deadly storm surge across the upper Texas and southwest Louisiana coasts that claimed dozens of lives [66].

Hurricane Ike in particular was chosen as a test case for this study because high levels of storm surge were generated and the fact that wave interaction in some areas resulted in up to 50% changes in modeled storm surge [29]. Thus, we know a-priori that the results from the SWAN model will have significant impacts on the accuracy of the resulting ADCIRC water levels and water velocities. More specifically, wave-induced set up from Ike is known to have been particularly large in the vicinity of the hurricane track and so we can expect a high sensitivity of the coupled wave-circulation output to the choices of source terms in the wave model.

### 3.2. Hurricane Ida

Hurricane Ida was a category 4 storm that made landfall on August 29, 2021 near Port Fourchon, Louisiana [19]. The storm had an intense wind field with sustained winds of over 150 mph causing billions of dollars in damage and several lives to be lost.

A main reason that Hurricane Ida was chosen as a second test case is because the storm produced large amounts of surge, recorded as high as 14 feet in some areas [5]. Additionally, the hurricane made landfall in a separate part of the Gulf of Mexico than Hurricane Ike, thus improving the robustness of our study to more than just a single case study. Additionally, because this storm is more recent there is ample data available to compare simulation results to. The data that will be used to evaluate errors in the model include NOAA gauge data for WSE and NOAA buoy data for wave statistics.

## 4. Implementation Details

### 4.1. Grids

The computational grid used in the Hurricane Ike scenario comes from the work of Kennedy et. al. and consists of 6,675,517 elements and 3,352,598 nodes with resolution ranging from the order of km in the deep ocean up to 20 m or less along the Texas coast where Ike made landfall [31]. Bathymetric data that defined the mesh was taken from a combination of satellite data sets and digital elevation models near the coast as specified in [31, 29].

For the Hurricane Ida scenario, a different mesh is used with high refinement specifically along the Louisiana coast. The mesh consists of 3,102,441 elements and 1,593,485 nodes with resolution in a similar range to that of the mesh used in Hurricane Ike. In this case, resolution around the Louisiana coast is as fine as 20 m while the remainder of the Gulf Coast has refinement of anywhere from the order of 100 m and deep ocean is as sparser on the order of km. The mesh for Ida is constructed from similar data sources to the Ike mesh. The mesh used for Ida is different than Ike because each mesh has particularly high resolution in the area where the storms made landfall, which is critical in achieving the accuracy of any circulation-wave model.

In both scenarios, the spectral domain for SWAN is 36 cells in direction,  $\theta$ , and 40 cells in frequency,  $\sigma$ . The directions have uniform spacing of  $10^\circ$  and range across the full circle,  $-180^\circ$  to  $180^\circ$  and the frequency goes from  $0.031384 Hz - 2.55 Hz$  with logarithmic spacing such that  $f_{i+1} = \gamma f_i$  where  $\gamma = 1.1$  is a constant. These specifications for the spectral grid may be slightly higher than operational forecast models but were chosen to allow for sufficient refinement of the SWAN model because the focus of this study is the impact of source term choices on the accuracy of the coupled wave-circulation model.

### 4.2. Forcing and Boundary Conditions

The input winds and pressure for the Hurricane Ike scenario are validated meteorology hindcasts from Ocean Weather Inc. (OWI). Because the OWI wind fields are not publicly available, the best track winds from the NHC's HURDAT2 dataset are used to force pressure and winds for the Hurricane Ida scenario [36]. This is also a similar wind format used during forecasting and thus provides an opportunity to assess a wind product used in such applications. HURDAT2 gives parametric information about the location and size of the hurricane and the Generalized Asymmetric Holland Model is used to approximate the actual wind and pressure fields that force ADCIRC+SWAN.

For both scenarios, conditions for the open ocean boundary at the  $60^\circ$  meridian for ADCIRC are generated from the TPXO global tide model [14]. To avoid inducing artificial oscillations into the simulation a 30 day tidal spin up of ADCIRC without winds and hence, no waves, is supplied as initial conditions to the ADCIRC+SWAN model in both scenarios. For Hurricane Ike, total simulation time is 8 days and 18 hours beginning on September 5, 2008 at 12:00 GMT and ending September 14, 2008 at 06:00 GMT. For Hurricane Ida the total run time is 9 days and 6 hours beginning at August 26, 2021 at 12:00 GMT and ending at September 4, 2021 at 18:00 GMT.

For the SWAN wave model, the initial conditions are set to 0 and the open boundary conditions for SWAN are 0.

**Table 1**

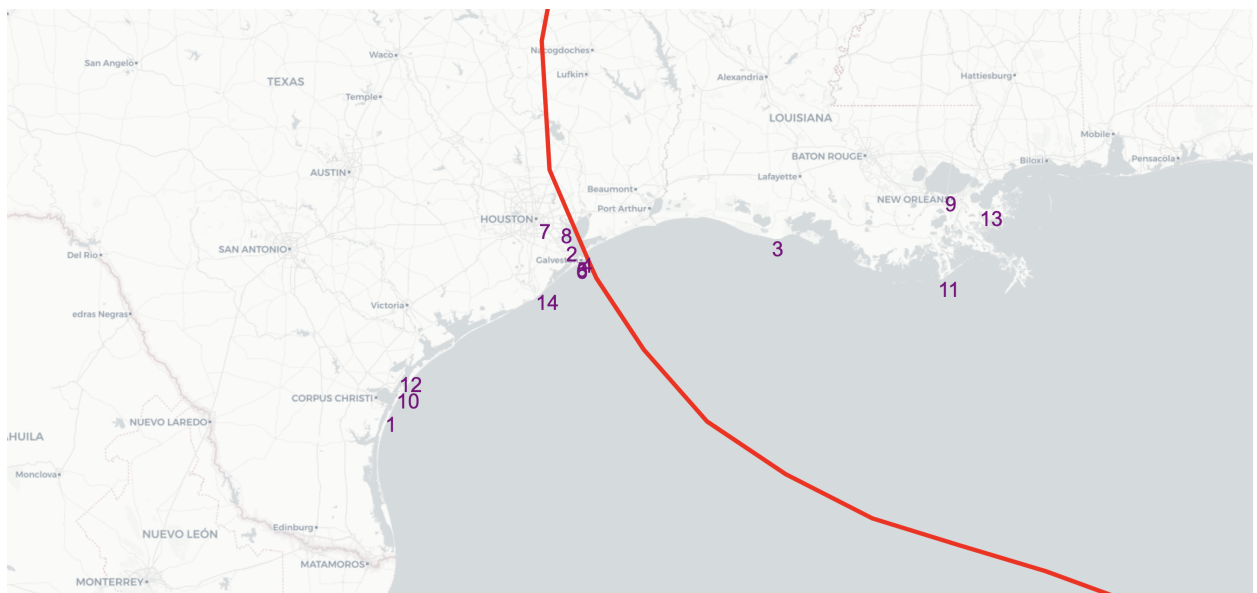
Water surface elevation stations used to compare ADCIRC+SWAN results for Hurricane Ike.

Gauge no.	Gauge Name	NOAA ID	Latitude	Longitude
1	Bob Hall Pier Corpus Christi	8775870	27.5800	-97.2167
2	Eagle Point	8771013	29.4813	-94.9172
3	Freshwater Canal Locks	8766072	29.5341	-92.3082
4	Galveston Bay Entrance North Jetty	8771341	29.3576	-94.7260
5	Galveston Pier 21	8771450	29.3100	-94.7933
6	Galveston Pleasure Pier	8771510	29.2849	-94.7894
7	Manchester Houston	8770777	29.7247	-95.2656
8	Morgans Point	8770613	29.6817	-94.9850
9	New Canal Station	8761927	30.0272	-90.1134
10	Port Aransas	8775237	27.8404	-97.0730
11	Port Fourchon	8762075	29.0848	-90.1985
12	Rockport	8774770	28.0217	-97.0467
13	Shell Beach	8761305	29.8681	-89.6733
14	USCG Freeport	8772447	28.9428	-95.3025

This study is conducted by running simulations of both Hurricane Ike and Hurricane Ida, each with identical forcing inputs while changing only the source term implementations in SWAN. ADCIRC is run without SWAN as a control and then 1st Generation (Gen1), 2nd Generation (Gen2), and the latest ST6 (Gen3) packages, as described in Section 4, are run. The coupling interval between ADCIRC and SWAN happens every 600 seconds for both scenarios.

### 4.3. Post Processing

The ensuing ADCIRC+SWAN water levels are compared to available measurements from NOAA gauges and significant wave height, mean wave period, and mean wave direction are compared to available NOAA buoys. A summary of the gauge locations for Hurricane Ike can be found in **Table 1** and can be seen on the maps in **Figure 1**. The gauge locations for Hurricane Ida can be found in **Table 2** and the locations can be seen on the map in **Figure 2**. A summary of the buoy locations used in both scenarios can be found in **Table 3** and their locations are shown on a map in **Figure 3**.

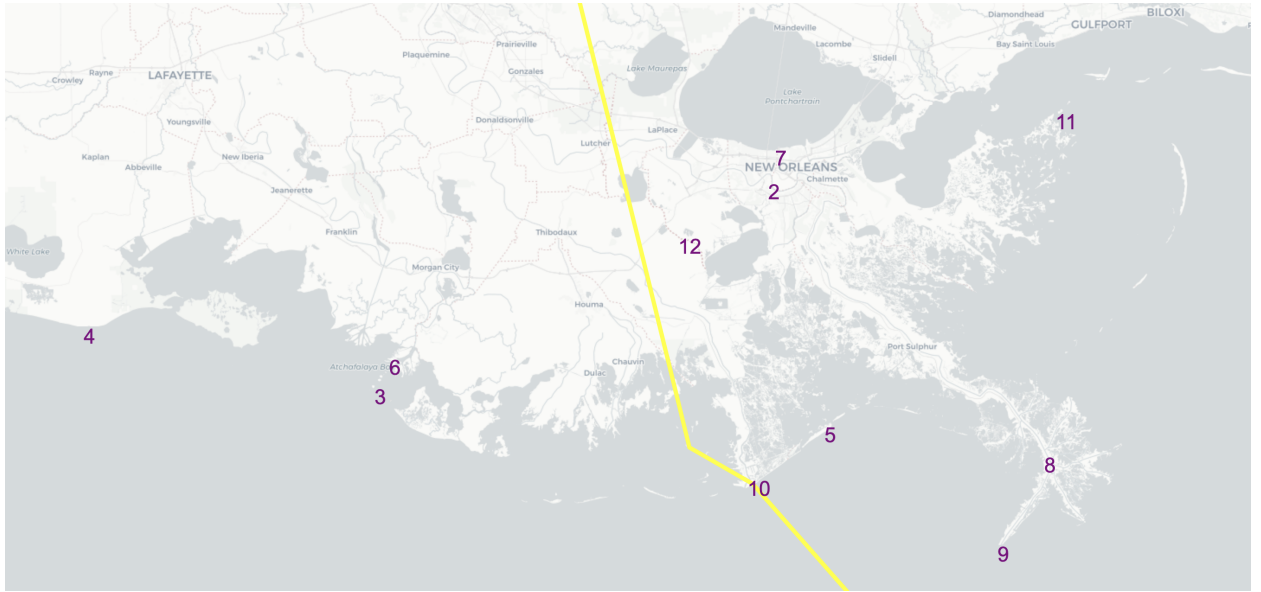


**Figure 1:** All water surface elevation gauges used during the Hurricane Ike test case. Hurricane Ike track in red.

**Table 2**

Water surface elevation stations used to compare ADCIRC+SWAN results for Hurricane Ida.

Gauge no.	Gauge Name	NOAA ID	Latitude	Longitude
1	Pilottown, LA	8760721	29.1793	-89.2588
2	Port Fourchon	8762075	29.1142	-90.1993
3	Shell Beach	8761305	30.1267	-89.2217
4	Grand Isle	8761724	29.2633	-89.9567
5	New Canal Station	8761927	30.0272	-90.1133
6	Freshwater Canal Locks	8766072	29.5341	-92.3082
7	LAWMA Amerada Pass	8764227	29.4500	-91.3383
8	Pilots Station East	8760922	28.9316	-89.4067
9	West Bank 1	8762482	29.7838	-90.4200
10	Eugene Island	8764314	29.3667	-91.3833
11	Bulk Terminal	8767961	30.1900	-93.300
12	Carrollton	8761955	29.9333	-90.1350
13	Calcasieu Pass	8768094	29.7683	-93.3433

**Figure 2:** Locations of NOAA water surface elevation gauges used to compare for Hurricane Ida. Hurricane Ida track in yellow.

The output from the ADCIRC+SWAN model records every 30 minutes at the locations of the gauges/buoys and errors at each station are computed while wind forcing is active to avoid biasing the results to when the contribution from wind waves is not active. This corresponds to computing the error during the 8 day and 18 hour period for Hurricane Ike and the 9 day and 6 hour period for Hurricane Ida as described in Section 4.2. The WSE from ADCIRC is compared to observations from the NOAA WSE gauges specified in **Tables 1,2** and the wave statistics from SWAN are compared to the observations from the NOAA buoys in **Table 3**. Two types of error are computed, root mean square error (RMSE) and the percent error of the peak value that are defined as:

$$e_{RMSE} = \sqrt{\frac{\sum_i (u_{i,sim} - u_{i,meas})^2}{N}} \quad (35)$$

$$e_{peak} = \frac{|\max(u_{sim}) - \max(u_{meas})|}{\max(u_{meas})} \times 100.$$

**Table 3**  
Wave buoy info.

Buoy no.	Buoy Name	Latitude	Longitude
1	NBDC 42035	29.2320	-94.4130
2	NBDC 42019	27.9100	-95.3450
3	NBDC 42001	25.9190	-89.6740
4	NBDC 42020	26.9680	-96.6930
5	NBDC 42002	26.0550	-93.6460
6	NBDC 42055	22.1240	-93.9410
7	NBDC 42040	29.2070	-88.2370
8	NBDC 42007	30.0900	-88.7690
9	NBDC 42039	28.7870	-86.0070
10	NBDC 42036	28.5010	-84.5080

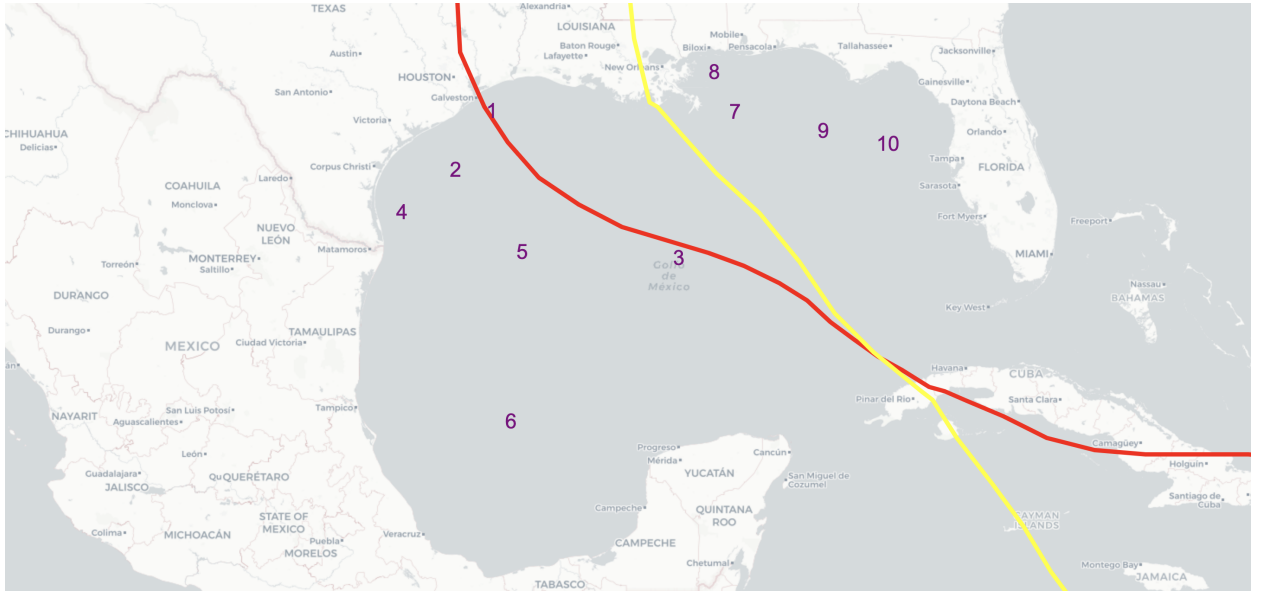


**Figure 3:** Wave buoy locations that are used in both of the scenarios. Hurricane Ike track in red and Hurricane Ida track in yellow.

The wave statistics that are recorded at the buoys are significant wave height, peak period, and mean wave direction. Significant wave height is defined as the highest 1/3 of recorded waves at a point, the peak period is the reciprocal of the frequency where the highest action density is recorded, and mean wave direction is as it sounds. In SWAN, the aforementioned statistical values must be estimated. The significant wave height is estimated by first calculating the zeroth moment of the spectrum,  $m_0$ . In general the  $i^{th}$  moment of the spectrum is defined as:

$$m_i(x, y) = \int_{-\pi}^{\pi} \int_{\sigma_{min}}^{\sigma_{max}} \sigma^i E(x, y, \sigma, \theta) d\sigma d\theta, \quad (36)$$

recall  $E = N\sigma$ . The significant wave height is estimated as:

$$H_s(x, y) \approx 4\sqrt{(m_0)}. \quad (37)$$

The reasoning behind this approximation to the highest one third of waves is not trivial but the derivation can be found in several texts, e.g., [28, 37]. The peak period is obtained just by finding the period in the spectrum that has the highest

**Table 4**

Wall clock times for ADCIRC+SWAN.

Model Configuration	Hurricane Ike Run Time (hr)	Hurricane Ida Run Time (hr)
No SWAN	1.094	0.647
Gen1	2.837	1.881
Gen2	2.688	1.818
Gen3	4.086	3.206

action density, and the mean wave direction in degrees is computed as:

$$\theta_{mean}(x, y) = \frac{180}{\pi} \frac{\int_{-\pi}^{\pi} \int_{\sigma_{min}}^{\sigma_{max}} \cos(\theta) E(x, y, \sigma, \theta) d\sigma d\theta}{\int_{-\pi}^{\pi} \int_{\sigma_{min}}^{\sigma_{max}} \sin(\theta) E(x, y, \sigma, \theta) d\sigma d\theta}. \quad (38)$$

## 5. Results

### 5.1. Computational Cost

Total wall clock times rounded to the nearest second are tabulated in **Table 4**. Each simulation is run in parallel with 1064 of the Intel Xeon Platinum 8280 ("Cascade Lake") processors distributed among 19 computational nodes on the Frontera supercomputer from the Texas Advanced Computing Center (TACC). The choice to use 1064 cores is because it has been found that scaling efficiency diminishes beyond around 2000 nodes per core. For the mesh used for Ike, this means 3150 nodes per core and for Ida, this amounts to 1497 nodes per core. For the Hurricane Ike scenario ADCIRC without SWAN coupling takes 1 hour and 5 minutes to run while the fastest ADCIRC+SWAN run is Gen2 with over double the run time at 2 hours and 41 minutes. Similarly, for Hurricane Ida the ADCIRC without SWAN took 38 minutes and 48 seconds while the fastest ADCIRC+SWAN run was with Gen2 at 1 hour 49 minutes and 3 seconds. Thus, we observe in both cases SWAN more than doubles the run time. This overhead is unsurprising because the number of parameters SWAN is solving for at each time step is 505 times larger than ADCIRC. This is because while ADCIRC is solving for 3 quantities (WSE and two velocity components) at each node on the mesh, SWAN is solving for the Action Balance on the whole spectral mesh ( $41 \times 37$  points) at each node in the finite element mesh. However, SWAN can take much longer time steps ( $\sim 10$  minutes) compared to ADCIRC ( $\sim 1$  second). Taking this into consideration, for each SWAN time step of 10 minutes we would expect ADCIRC to have 600 forward solves. Therefore, over the course of a given simulation we would expect SWAN to solve for about  $505/600 \approx .85$  times the variables ADCIRC must solve for. In other words, if SWAN were able to solve for each of its unknowns as quick as ADCIRC could, we would expect ADCIRC+SWAN to take 1.85 times the time of ADCIRC by itself. From **Table 4** we can see that for any source term package in SWAN it takes considerably longer than 1.85 times just ADCIRC. Thus we can conclude that either SWAN takes longer to solve per unknown than ADCIRC (that would be unsurprising because SWAN solves implicitly while ADCIRC is explicit), there is other associated overhead with running SWAN, such as computation of specific source terms, or a combination of both.

Another interesting part of the results in **Table 4** is the large difference in run times due to the choice of source term package. It was observed that running ADCIRC+SWAN with Gen3 source terms took around 1.5 times longer than either Gen1 or Gen2. A plausible explanation for the increased run time is the computational complexity of the Gen3 source terms due to the inclusion of the DIA, the approximation for the four wave nonlinear interactions, as well as the LTA for three wave interactions. This could merit further investigation to confirm this intuition but at this time we cannot say for sure this is the sole reason for changes in run time because there are many source terms that change between the 1st/2nd gen and 3rd gen set ups besides just the DIA and LTA. Additionally, it isn't surprising to see that Gen2 and Gen1 didn't have significantly different run times (only a 5% difference) because the only difference between the two is the definition of a single parameter as defined in (33).

### 5.2. ADCIRC Output

During the Hurricane Ike simulation, the data from the 14 NOAA gauges along the Texas coast (see **Figure 1**), and the output WSE from ADCIRC+SWAN are used to compute the errors,  $e_{RMSE}$  and  $e_{peak}$  as in (35). The error statistics are plotted in bar graphs to compare the 4 configurations (No SWAN, 1st Gen, 2nd Gen, 3rd Gen) in **Figure 4**. Similarly, during the Hurricane Ida simulation, the 13 NOAA gauges along the Louisiana coast (see **Figure 2**), and the

output WSE from ADCIRC+SWAN are used to compute the errors which are plotted for all of the 4 configurations in **Figure 5**. During Hurricane Ike, the average RMSE across all gauges when excluding waves altogether is 0.210 meters while for Gen1 it is .190 m, Gen2 is .196 m, and Gen3 is .197 m. During Hurricane Ida, the average RMSE across all gauges when excluding waves altogether is 0.285 meters while for Gen1 it is .282 m, Gen2 is .281 m, and Gen3 is .282 m.

Including waves resulted in less than a 5 percent reduction in RMSE during Hurricane Ike and less than 1.5 percent during Hurricane Ida at the gauge locations. The choice of source terms really did not impact RMSE with only a maximum difference of .007 m between Gen1 and Gen3 during Hurricane Ike and a maximum difference of .001 m between Gen2 and Gen3. The absolute average relative error percent to the peak value without accounting for waves is about 13 percent while Gen1 is 12 percent, Gen2 is 10 percent, and Gen3 is 11 percent during Hurricane Ike. For Hurricane Ida, the same quantity is 20 percent without waves while Gen1 is 20 percent, Gen2 is 21 percent, and Gen3 is 22 percent. Qualitatively examining the outputs in the graphs of **Figure 4** and **Figure 5** does not show any drastic improvements in accuracy between one source term package over the others across all the gauge locations and during Hurricane Ida it doesn't appear that including waves reduces the error compared to the NOAA WSE gauge data overall. This is not to say including waves does not improve the overall quality of the simulation.

We can see that outside of analyzing the accuracy of time series WSE data at the gauge locations, there is a large sensitivity to global ADCIRC+SWAN WSE levels due to source term configuration within SWAN. In **Figure 6** we have plotted the differences in the maximum recorded WSE from ADCIRC+SWAN of the various source term configurations during Hurricane Ike, and we have the same quantities plotted for Hurricane Ida in **Figure 7**. For Hurricane Ike, it can be seen that excluding waves altogether leads to a reduction of max WSE of nearly 0.5 m near the coastline (**Figure 6**, top right) and for Ida we see similar results with the exclusion of waves reducing max WSE near the coastline by nearly 0.5 m (**Figure 7**, top right).

For Ike, it appears that the max WSE of the 3rd gen simulation is nearly 0.1 m less on average in the vicinity of the coast when compared to both 1st and 2nd gen simulations (**Figure 6**, top left and bottom right respectively). For Ida, it appears that the max WSE of the 3rd gen simulation varies strongly spatially and on average the max WSE seems to be higher than both 1st and 2nd gen simulations, though there are significant regions near the track of Ida where the 1st and 2nd gen have higher max WSE compared to 3rd gen (**Figure 6**, top left and bottom right respectively). We can also see there are differences in max WSE between the reduced order source terms in both Ida and Ike, though much smaller in magnitude than between any of the other simulations (**Figure 6** and **Figure 7**, bottom left).

### 5.3. SWAN Output

The significant wave height, peak period, and mean wave direction of the ADCIRC+SWAN simulations are used to compute the errors relative to the 10 available NOAA wave buoys from **Figure 3** and plotted as bar graphs for Hurricane Ike in **Figure 8** and **Figure 9** for Hurricane Ida.

The average RMSE for significant wave height across all stations for Gen1 is 0.900 m, Gen2 is 1.033 m, and Gen3 is 0.802 meters during Hurricane Ike and .813 m for Gen1, 0.883 for Gen2, and 0.834 for Gen3 during Hurricane Ida. During the Hurricane Ike case we do see a 10 percent improvement in RMSE from Gen1 to Gen3 and a roughly 20 percent improvement in error from Gen2 to Gen3 at the buoy locations while during Hurricane Ida we see that Gen1 has the lowest average RMSE but all source term packages are within 0.07 m in average RMSE. The absolute average error percentage relative to the peak value of the buoy was 27 percent for Gen1, 30 percent for Gen2, and Gen3 was 22 percent for Hurricane Ike and for Hurricane Ida was 40 percent for Gen1, 81 for Gen2, and 63 for Gen3. During Hurricane Ike, much of the difference in the errors between the 3 source term packages was due to buoy number 6 (NBDC 42055) where both Gen1 and Gen2 nearly doubled the observed peak significant wave height while Gen3 only underpredicted by 2 percent. During Hurricane Ida, it appears that the significant wave height significantly over-predict the observed data except in case of buoys 7,9, and 10 regardless of source term package.

The average RMSE for peak period across all buoys for Gen1 was 2.822 seconds, Gen2 was 2.541 seconds, and Gen3 was 2.413 seconds for Hurricane Ike and 4.865 seconds for Gen1, 5.068 second for Gen2, and 9.960 seconds for Gen3 during Hurricane Ida. During Hurricane Ike we do see improved accuracy relative to these 10 buoys as we upgrade in complexity of source terms from Gen1 to Gen2 to Gen3, with a maximal improvement of about 15 percent in error reduction. The absolute average across all buoys of the relative error percentage of the peak is 10 % for Gen1, 8 % for Gen2, and 14 % for Gen3. For Hurricane Ida we find no such improvement with more complex source terms and in fact Gen3 performs significantly worse when compared to buoys.

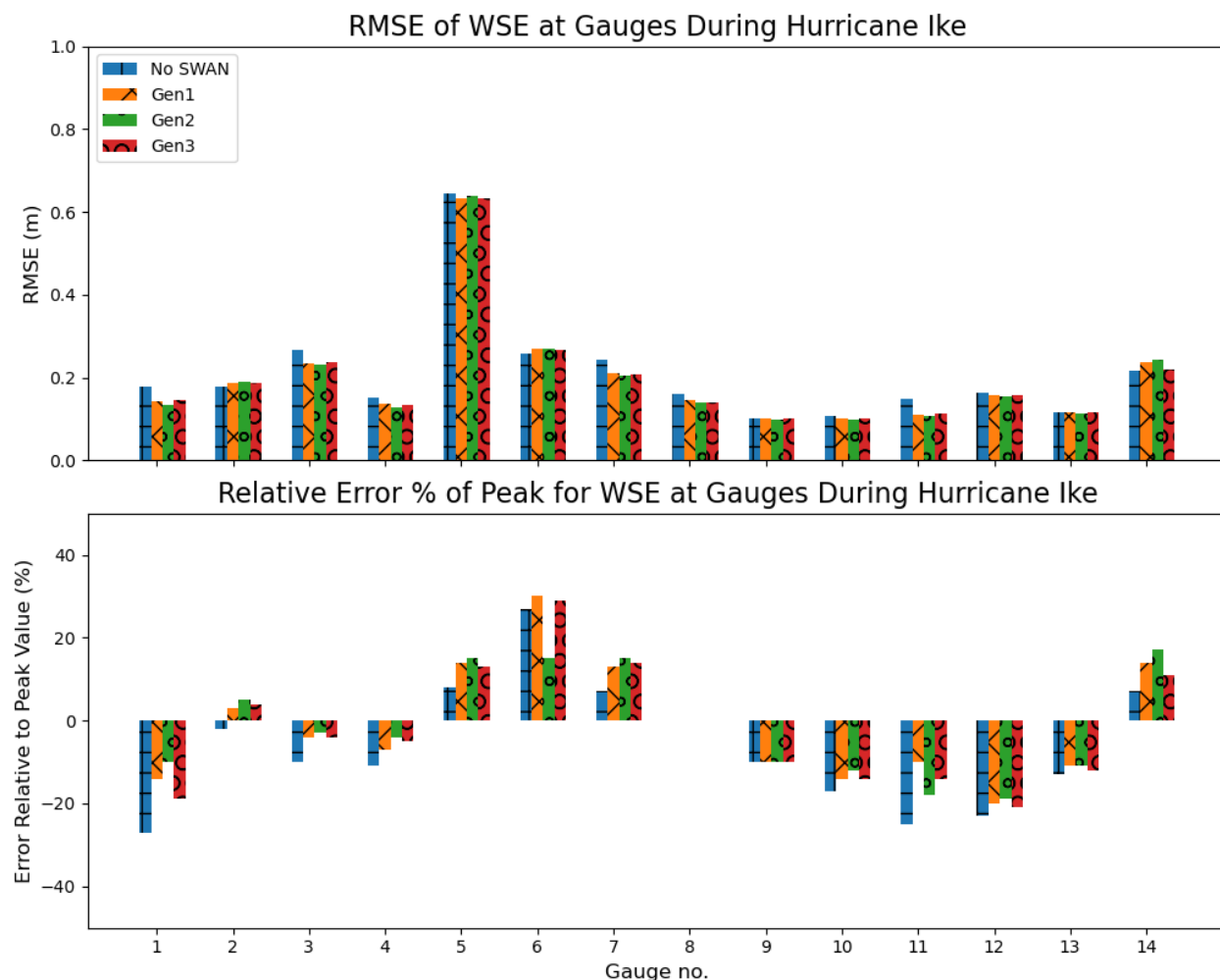


**Figure 4:** Error statistics relative to NOAA gauge data for Hurricane Ike simulation.

The average RMSE for mean wave direction across all buoys is 43.238 degrees for Gen1, 40.392 degrees for Gen2, and 37.076 degrees for Gen3 during Hurricane Ike and 62.380 degrees for Gen1, 60.229 degrees for Gen2, and 67.73 degrees for Gen3 during Hurricane Ida. During Hurricane Ike, the more complex source terms in Gen3 do improve the RMSE over the buoys and in this case by roughly 14 percent relative to Gen1. The absolute average across all buoys of the relative error percentage to the peak buoy value is 23 % for Gen1, 30 % for Gen2, and 17 % for Gen3. However, no such improvements are observed during Hurricane Ida.

The larger errors in some of the SWAN output with respect to buoys are most likely related to the inaccuracy of the wind fields, particularly during Hurricane Ida. Because the best track winds were used for Hurricane Ida, this results in a highly simplified wind field that doesn't capture the highly irregular oscillations that are observed by the buoys as shown in **Figure 11**. The average RMSE in wind magnitude across all buoys is roughly 5 m/s during Hurricane Ida while it is only around 2 m/s during Hurricane Ike. A comparison between wind velocity magnitude of the ADCIRC simulation and the buoy data during Hurricane Ike is shown in **Figure 10**.

We can also look at global sensitivity of the wave statistics outputs in ADCIRC+SWAN related to the choice of source terms. In **Figure 12** we can see the differences in maximum significant wave height due to changes in the source term configurations for both Ike and Ida simulations. We can see that during Ike, the significant wave height globally seems to be lower in the deep ocean when compared to 1st or 2nd gen but near the coast and near the hurricane track the 3rd gen has maximum significant wave heights that are a meter or more higher than the reduced order scenarios (**Figure 12**, top left and bottom left). During Hurricane Ida, it is interesting to see that near the track the max significant

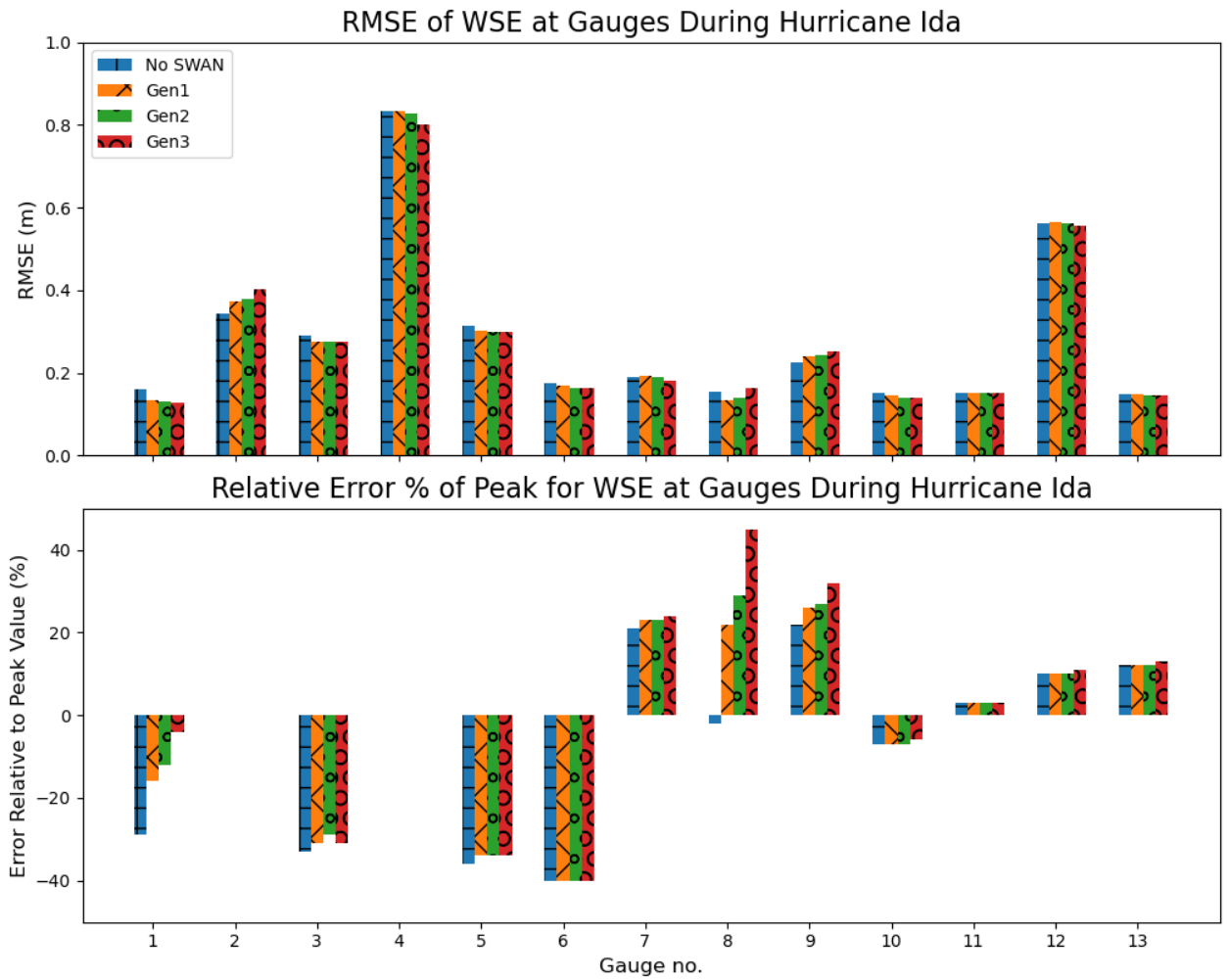
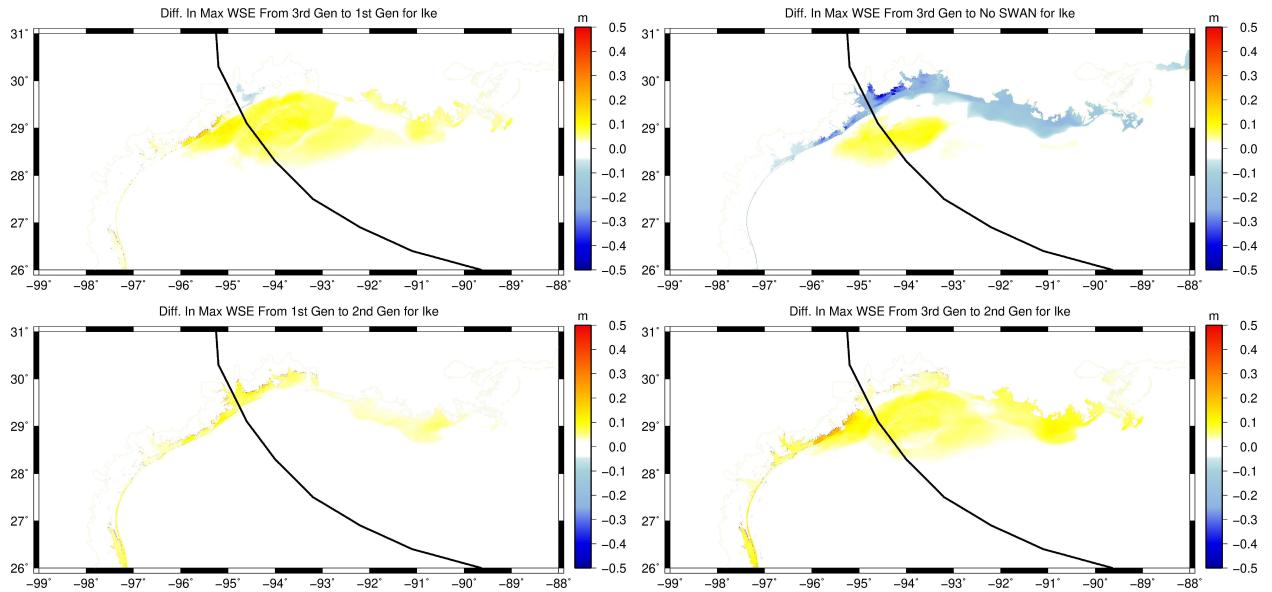
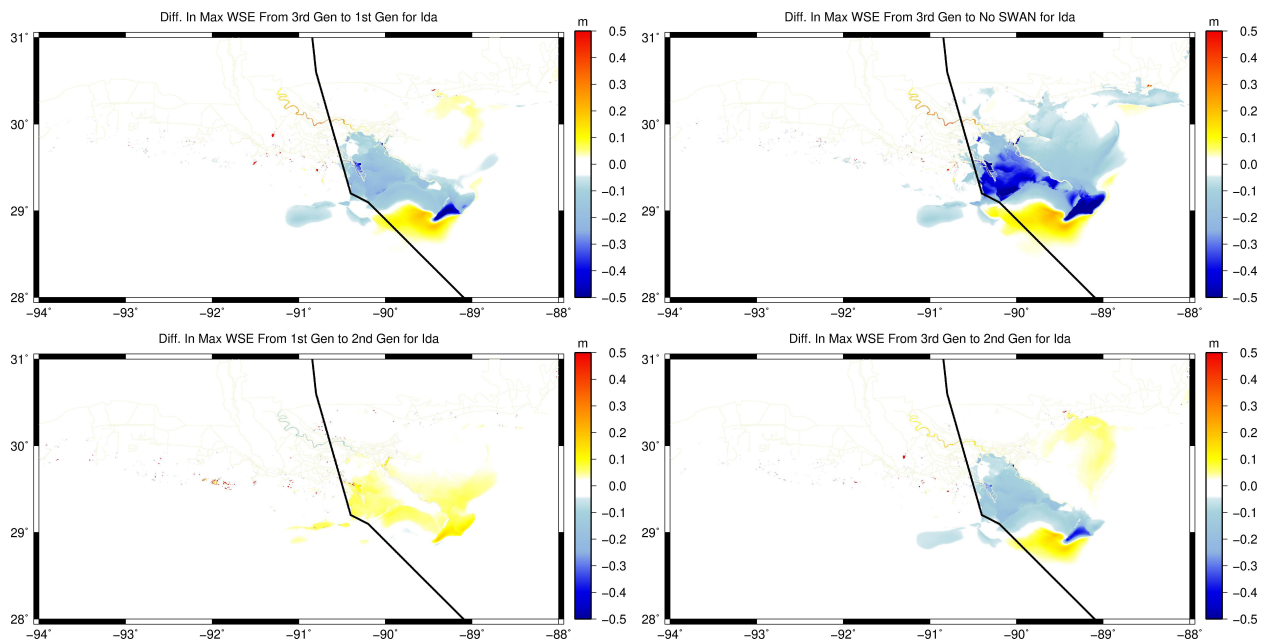


Figure 5: Error statistics relative to NOAA gauge data for Hurricane Ida simulation.

wave height is multiple meters higher for the 3rd gen than either the 1st or 2nd gen scenarios (Figure 12, top right and bottom right).



**Figure 6:** Differences between maximum water surface elevation due to choices of source term package. **Top left:** Max WSE of 1st Gen minus max WSE of 3rd Gen. **Top right:** Max WSE of No SWAN minus max WSE of 3rd Gen. **Bottom left:** Max WSE of 2nd Gen minus max WSE of 1st Gen. **Bottom right:** Max WSE of 2nd Gen minus max WSE of 3rd Gen.



**Figure 7:** Differences between maximum water surface elevation due to choices of source term package. **Top left:** Max WSE of 1st Gen minus max WSE of 3rd Gen. **Top right:** Max WSE of No SWAN minus max WSE of 3rd Gen. **Bottom left:** Max WSE of 2nd Gen minus max WSE of 1st Gen. **Bottom right:** Max WSE of 2nd Gen minus max WSE of 3rd Gen.

Efficacy of reduced order source terms for a coupled wave-circulation model in the Gulf of Mexico

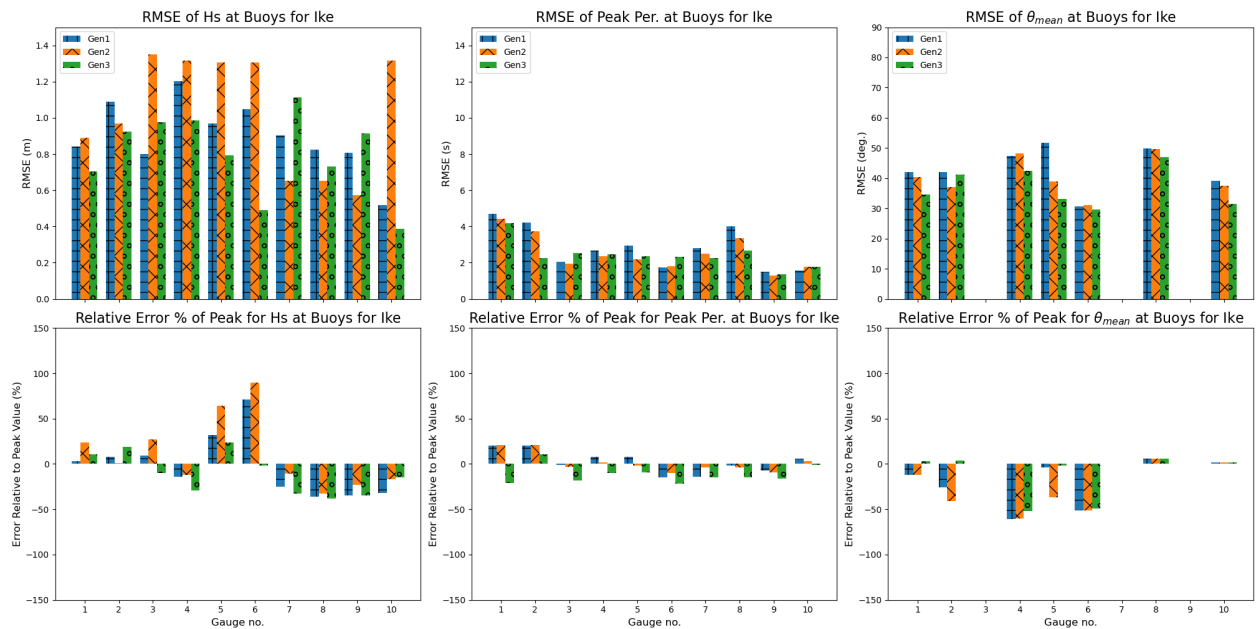


**Figure 8:** Error statistics relative to NOAA buoy data for Hurricane Ike simulation for significant wave height, peak period, and mean wave directions.

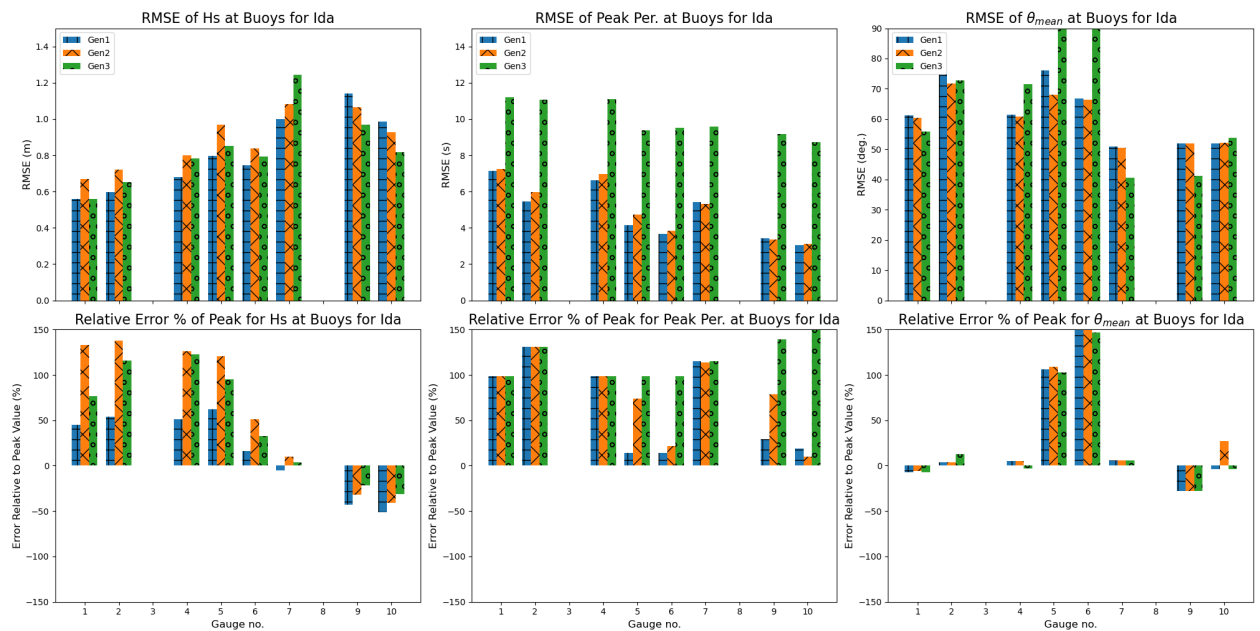


**Figure 9:** Error statistics relative to NOAA buoy data for Hurricane Ida simulation for significant wave height, peak period, and mean wave directions.

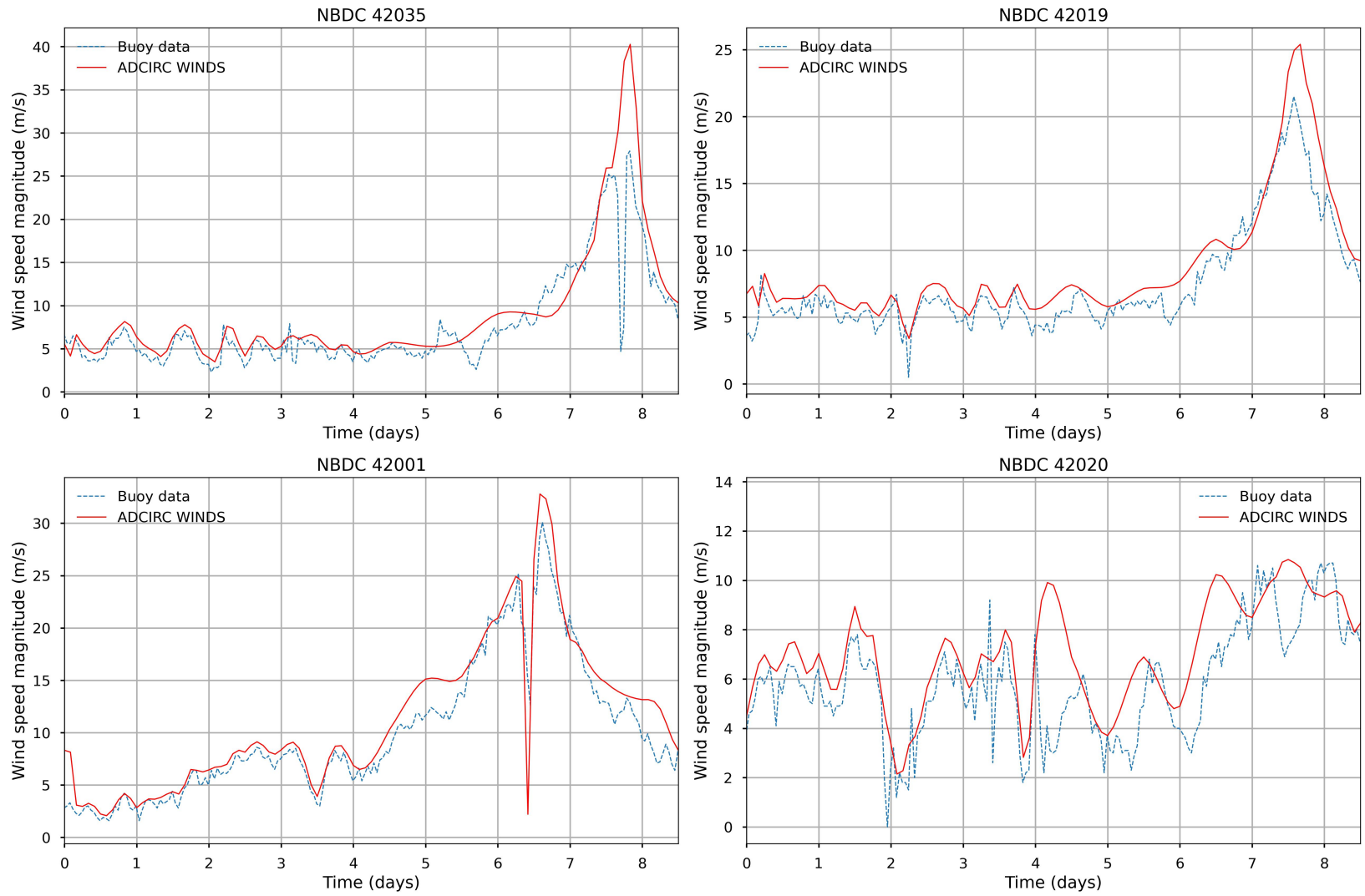


Figure 10: Wind velocity magnitude of NOAA buoys 1-4 along with ADCIRC+SWAN wind forcing during Hurricane Ike .

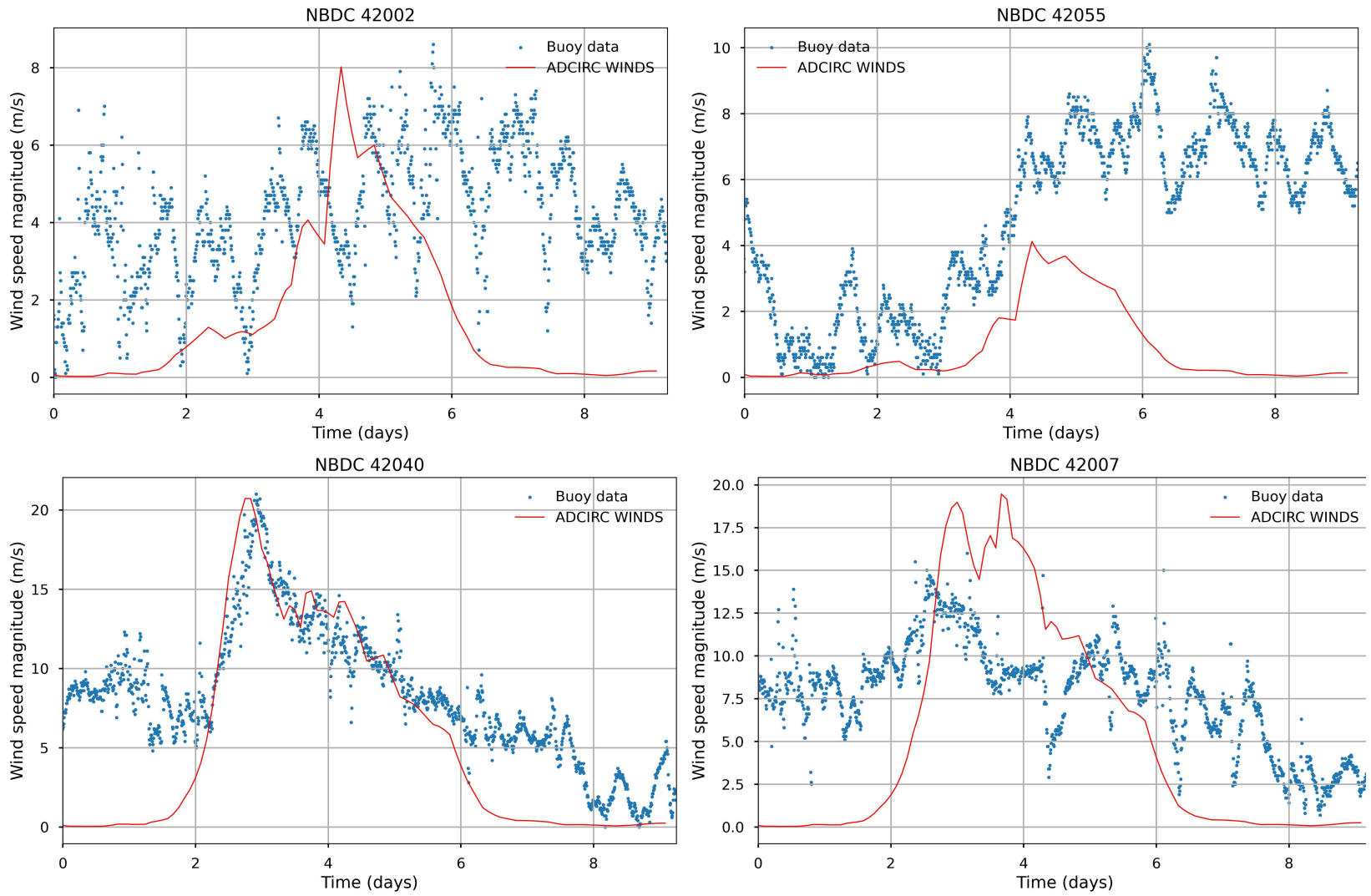
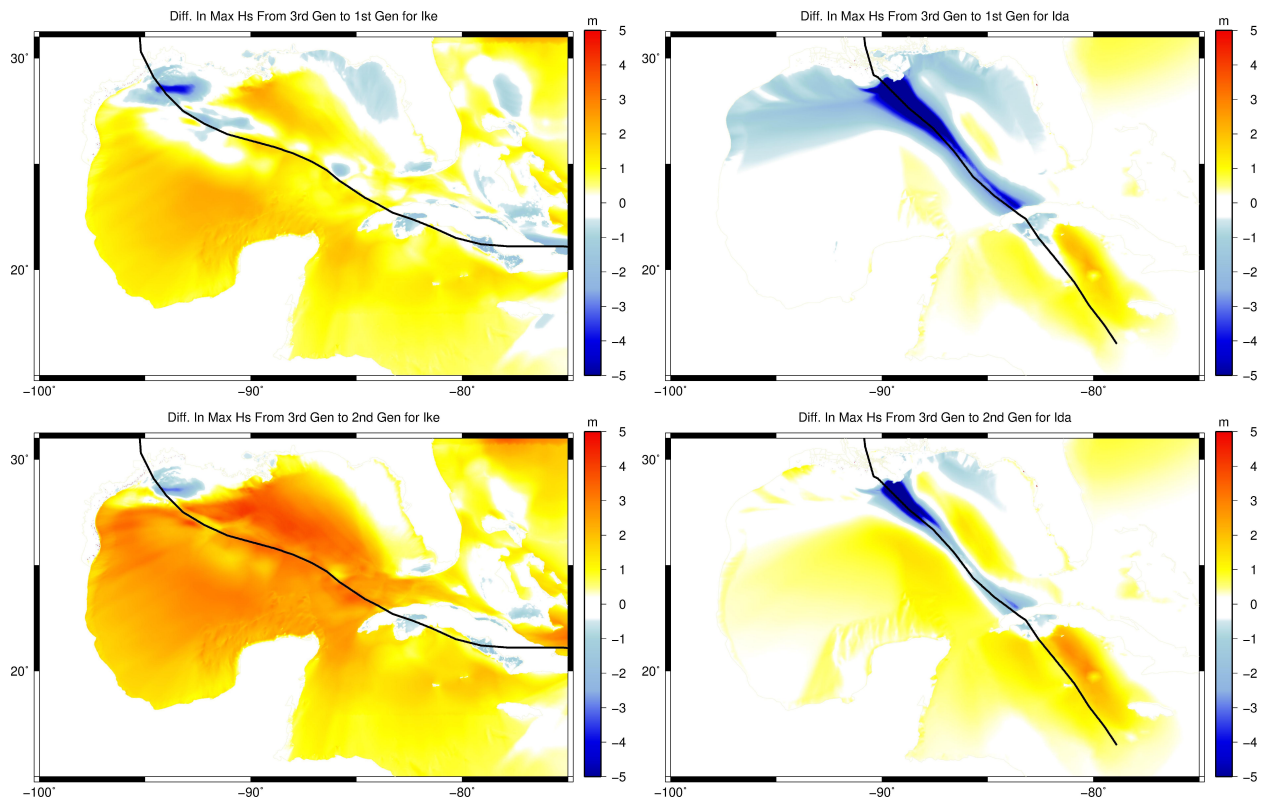


Figure 11: Wind velocity magnitude of NOAA buoys 5-8 along with ADCIRC+SWAN wind forcing during Hurricane Ida.



**Figure 12:** Differences between maximum significant wave heights due to choices of source term package. **Top left:** Max Hs of 1st Gen minus max Hs of 3rd Gen for Ike. **Top right:** Max Hs of 1st Gen minus max Hs of 3rd Gen for Ida. **Bottom left:** Max Hs of 2nd Gen minus max Hs of 3rd Gen for Ike. **Bottom right:** Max Hs of 3rd Gen minus max Hs of 3rd Gen for Ida.

## 6. Conclusions

From this study, it was observed that varying the source term packages in SWAN as part of a validated ADCIRC+SWAN model significantly impacted run times as well as results in wave outputs. Upgrading from Gen1 or Gen2 source terms to the ST6 Gen3 source terms resulted in about a 40 percent increase in run time. The effects of the choice of source terms (Gen1, Gen2 or Gen3) on average WSE at NOAA gauges only changed RMSE relative to the gauges by about .007 m. However, more significant differences in wave statistics were observed at the NOAA buoy locations based on source term choice. These differences greatly depended on the scenario, as during Hurricane Ike Gen3 source terms showed roughly a 20 percent improvement in the accuracy of significant wave height, and a 15 percent improvement in accuracy of peak period, and a 14 percent improvement in accuracy mean wave direction relative to Gen1 or Gen2 source terms while during Hurricane Ida no such improvements in accuracy were observed.

This study shows the possible trade-off between accuracy and run time for the choice of source term complexity in SWAN in the coupled ADCIRC+SWAN setting. The small differences in accuracy compared to observed water levels of the source term configurations may warrant more investigation into the use of reduced order source packages such as Gen1 or Gen2. For instance, it may be worth the savings in computation if only water surface elevations are of primary interest as opposed to wave statistics. However, large sensitivities to the source term choice in global output of significant wave height near hurricane tracks were observed. A key observation from this study is that if the meteorological forcing isn't highly accurate, which is common in forecasting scenarios, then the additional computational cost associated with the highly detailed Gen3 source terms may not improve accuracy of the model. Additionally, the computational savings shown when using the reduced order source terms could allow for potentially higher spectral resolutions to be used.

Some limitations of this study is that this was for a single geographic region, only two storm were run, and the source terms were not specifically tuned for this region so these results may vary significantly for a different domain or accuracy of the wave model could be improved if the source terms were tuned specifically for this region.

## Acknowledgements

This work has been supported by the United States Department of Homeland Security Coastal Resilience Center research project "Accurate and Fast Wave Modeling and Coupling with ADCIRC". The authors also would like to gratefully acknowledge the use of the "DMS23001" and "DMS21031" allocations on the Frontera supercomputer at the Texas Advanced Computing Center at the University of Texas at Austin.

## A. Source Terms Overview

### A.1. Historical Context

Operational wind wave models date back to the 1960s and 1970s and had success in many cases [30]. However, there were many issues with the evolution of the spectral shape and there were large discrepancies from model to model due to differences in source term configurations [53]. In the 1970s the sea wave modeling project (SWAMP) was conducted to review, analyze, and compare problems among operational wind wave models. In the review, spectral wind wave models were categorized into three generations based on how the models treat source terms [53]. The categorization is still used commonly in the wave modeling community and can be summarized in the following way.

First generation wave models are those that either have no source term explicitly accounting for nonlinear wave-wave interactions or the source term implemented for nonlinear wave-wave interactions is insignificant in magnitude compared to wind input. The first generation models had success in modeling certain scenarios but in general were found to underestimate observed wave growth and required tuning of the source term for wind input,  $S_{in}$ , to an extent that was shown to be non-physical [32]. Furthermore, the first generation models were unable to explain what is known as "the overshoot phenomenon" of a growing wind sea. With respect to the wind wave models, the overshoot effect results in the rapid growth of wave energy on the forward (low frequency) face of the spectrum (see **Figure 13**) [32]. The work by Hasselmann *et al.* both with theory and the important JONSWAP experiment led to consensus that this overshoot effect is a real phenomenon that is driven primarily by nonlinear wave-wave interaction [20, 21].

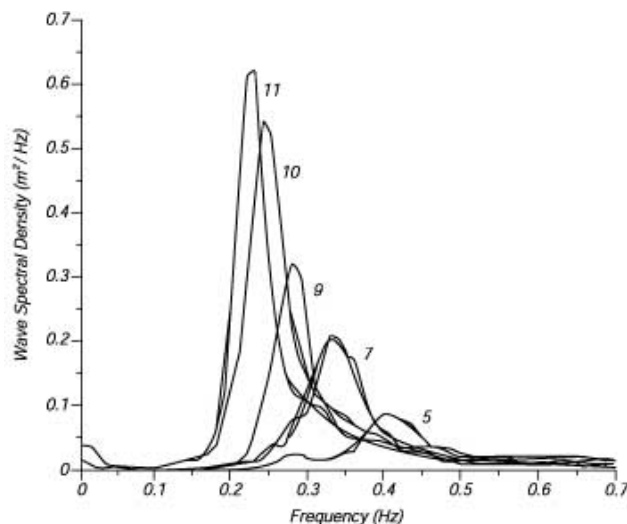


**Figure 13:** Data collected from JONSWAP experiment [20]. Shows overshoot effect from nonlinear interactions causing spectrum to shift from high frequencies (5) to low frequencies (11) as sea state develops. Figure from <https://wikiwaves.org>.

To address the nonlinear interactions as illustrated above, second and third generation wind wave models were developed. Second generation models are those with nonlinear source terms  $S_{nl}$  that are defined in terms of a small number of parameters. Within the second generation model category there are two different kinds of models, referred to as 'coupled hybrid' and 'coupled discrete'.

The coupled hybrid models are those that separate the treatment of the wind sea and the swell (see **Figure 14**). For the wind sea, the dynamics are treated parametrically and assume a certain spectrum shape a-priori to account for nonlinear interaction. The swell portion of the spectrum is treated by using a similar approach to the first generation models but neglecting nonlinear effects. According to the SWAMP study, the hybrid models have difficulties in the transition zone of the spectrum between wind sea and swell where the nonlinear effects still play a role. The coupled

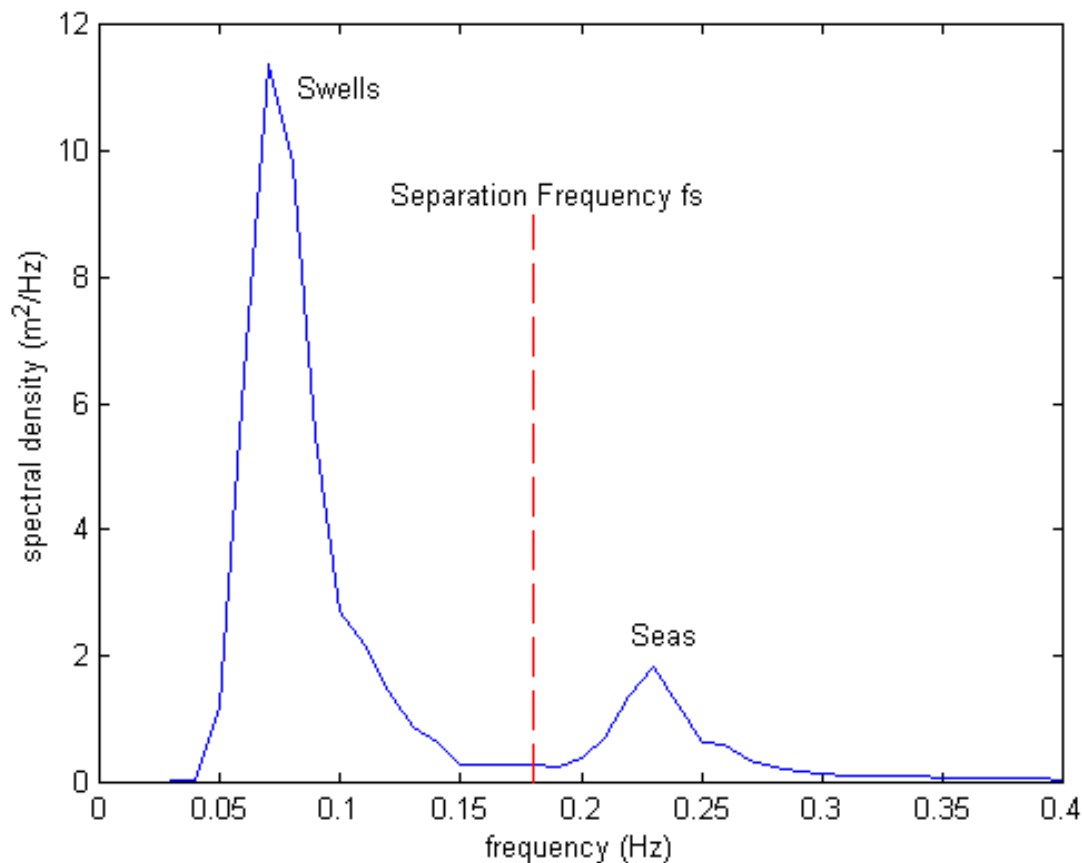


**Figure 14:** A typical wave spectrum that shows the wind sea and the swell. Figure from noaa.gov.

discrete models attempt to address this issue in the transition zone by representing both wind sea and swell components of the spectrum without parameterizing the wind sea component. However, the nonlinear interactions are still highly simplified into a parametric form. The SWAMP study argued that simplifying the nonlinear interactions restricts the spectral shapes the coupled discrete model can take on. Furthermore, coupled discrete models had documented problems with stability and generating unrealistic spectrum shapes [53].

As a result of the inconsistencies, the SWAMP study called for a new class of wind wave models deemed third generation models. Beginning in the 1980s and continuing through the 1990s, many operational models based on this third generation paradigm were developed. Some popular examples of third generation wind wave models that are still widely used operationally are SWAN, WAVEWATCH III, WWM III and WAM [6, 55, 51, 34]. Third generation models are different from first and second generation models in that they explicitly approximate the full nonlinear interaction in  $S_{nl}$ . Third generation models for the most part are still the common form of wind wave model.

There are many specific forms of the source terms that third generation models have employed. For this study, the third generation model in use will be SWAN and the latest available package will be used that is considered the state of the art and often referred to as the ST6 source terms [49]. It is also worth noting that ST4 source terms are still often used and have shown promising results [59].

It is also important to note that within the third generation models, the reliance on a significant approximation to the nonlinear interactions,  $S_{nl}$ , is necessary for the model to be scalable. In this study the Discrete Interaction Approximation (DIA) will be used that is the most commonly used in operational models [25]. There has been recent work on improving this approximation to nonlinear wave-wave interactions with other methods like Gauss quadrature method (GQM), the two scale approximation (TSA) [48], Generalized Multiple DIA [56], and the RIAM method [33].

## A.2. Wind Input $S_{in}$

In the 1950s there were two popular theories on wave generation from winds that emerged, one by Phillips and one by Miles [46, 43]. These general theories were adapted and put into a form that is compatible with the Wave Action Balance Equations. The theory of Phillips describes monochromatic waves generated from resonance caused by fluctuations in pressure over the ocean surface due to wind that results in a linear growth term [45]. The theory of Miles considers the change in air flow due to the presence of existing waves, resulting in a feedback mechanism and in an exponential growth term [45]. Most operational models to this day use a sum of both the linear growth from the theory of Phillips and the exponential growth from the theory of Miles to define source term  $S_{in}$  that is of the abstract form:

$$S_{in} = \alpha + \beta E(x, y, \sigma, \theta, t). \quad (39)$$

Here  $\alpha$  would be some coefficient representing the linear wave growth due to the theory of Phillips and  $\beta E(x, y, \sigma, \theta, t)$  represents the exponential wave growth due to the theory of Miles. A full derivation of  $S_{in}$  in the above form can be found in many text books [28, 34, 63]. These two theories can be thought of as constitutive relations that allow for the complex phenomenon of turbulent flow of the air at the ocean surface generating waves to be written in closed form. There has been documented disagreement between the theories of Phillips and Miles with laboratory and field experiments in addition to doubts on the validity of drag coefficients during extreme weather events [1]. However, these theories can produce reasonable results in observational wind wave models and variations of that are still used in popular wind wave models such as SWAN [6], WAVEWATCH III [57], MIKE21 [60], and WAM [34].

The model in this dissertation will use the default 3rd generation source term package used in SWAN cycle III Version 41.41 [54]. The default wind input term is that from WAM Cycle III and first outlined in [35]. The input term is defined as in (14) with  $\alpha = 0$  and  $\beta$  defined as:

$$\beta = \max(0, 0.25 \frac{\rho_{air}}{\rho_{water}} (28 \frac{u_*}{c} \cos(\theta - \theta_{wind}) - 1)) \sigma, \quad (40)$$

$\rho_{air}$  is the density of the air that is by default set to  $1.225 \frac{kg}{m^3}$ .  $\rho_{water}$  is the density of water that by default is set to  $997 \frac{kg}{m^3}$ .  $c$  is the phase velocity that is a consequence of the dispersion relation from (8).  $\theta$  is the direction that is an independent variable.  $\theta_{wind}$  is the mean wind direction.  $\sigma$  is the relative radian frequency that is another one of the independent variables.  $u_*$  is known as the friction velocity and is defined as follows:

$$u_*^2 = U_{10}^2 C_D. \quad (41)$$

Here  $U_{10}$  is the relative wind speed at 10 meters above the surface of the ocean, this is commonly used in operational ocean models. It is important to note that in the presence of ambient currents,  $U_{10}$  is defined as the wind speed minus the current vector.  $C_D$  is the drag coefficient and is taken from a study by Wu et.al. 1982 [62]:

$$C_D = \begin{cases} 1.2875 \times 10^{-3} & U_{10} < 7.5 m/s \\ (0.8 + 0.065 U_{10}) \times 10^{-3} & U_{10} \geq 7.5 m/s. \end{cases} \quad (42)$$

The default SWAN actually uses a second order polynomial fit to better account for empirically observed drop off of wind growth at higher wind speeds that isn't accounted in the model from Wu [54]. In this case  $C_D$  is set as:

$$C_D = (0.55 + 0.297 \frac{U_{10}}{U_{ref}} - 1.49 (\frac{U_{10}}{U_{ref}})^2) \times 10^{-3}. \quad (43)$$

$U_{ref}$  is the reference wind speed that is by default set at  $31.5 \frac{m}{s}$ . In the last decade or so beginning with the work of Ardhuin, Babanin and many others, the state of the art source term package has changed to become semi-empirical in

an aim to agree better with observed data and specifically to be more robust to situations with extreme weather [3]. This work culminated into new source terms for  $S_{in}$  and  $S_{wc}$ , and is often referred to as ST6 that was first fully defined in a paper by Rogers et. al. 2012 [49]. This source term package is available and widely used in both SWAN and WAVEWATCH III. The wind input term for the ST6 package is defined as follows,  $\alpha = 0$  and  $\beta$  from (14) is:

$$\beta = \gamma \sigma \frac{\rho_{air}}{\rho_{water}}, \quad (44)$$

where  $\gamma$  is a parameter that depends on location, direction, and frequency as:

$$\gamma(x, y, f, \theta) = G(x, y, f, \theta) \sqrt{B_n(x, y, f)} W(x, y, f, \theta). \quad (45)$$

In this context  $f = \frac{\sigma}{2\pi}$  and  $G, B_n, W$  are defined as follows:

$$G = 2.8 - (1 + \tanh(10 \sqrt{B_n(x, y, f)} W(x, y, f, \theta) - 11)), \quad (46)$$

$$B_n(x, y, f) = \frac{A(x, y, f)}{2\pi} E(x, y, f) k^3 c_g, \quad (47)$$

$$W(x, y, f, \theta) = (\max(0, \frac{U_{10}}{c} \cos(\theta - \theta_{wind}) - 1))^2. \quad (48)$$

In this case  $E(x, y, f)$  is the integrated spectrum  $E(x, y, f) = \int_{\theta} E(x, y, f, \theta) d\theta$ , where  $E(x, y, f, \theta) = E(x, y, \sigma, \theta) 2\pi$ .  $c_g$  is the group velocity as previously defined in (10).  $A(x, y, f)$  is the wave steepness defined by:

$$\frac{1}{A(x, y, f)} = \int_{\theta} E_n(x, y, f, \theta) d\theta. \quad (49)$$

Where  $E_n(x, y, f, \theta)$  is  $\frac{E(x, y, f, \theta)}{E'(x, y, f)}$  and  $E'(x, y, f)$  is:

$$E'(x, y, f) = \max_{\theta} (E(x, y, f, \theta)). \quad (50)$$

To be clear, the SWAN default  $S_{in}$  is a modification on the WAM Cycle 3 terms as defined in (40) - (43) while the ST6  $S_{in}$  described in (44) - (50) terms are considered the state of the art and used in this study.

### A.3. Dissipation $S_{diss}$

The change in variance density due to dissipation,  $S_{diss}$ , can take many forms depending on that wind wave model is being discussed. Changes in the spectrum due to dissipation are still not well understood, in fact according to the proceedings of a recent conference on wind waves, "Theoretical and experimental knowledge of the spectral wave dissipation is so insufficient that, to fill the gap, spectral models have been used to guess the spectral dissipation function as a residual term of tuning the balance of better known source functions to fit known wave spectrum features" [1]. In general,  $S_{diss}$  is separated as a sum of several terms that can include wave breaking in deep water (whitecapping), bottom friction, and depth-induced breaking. There are many other dissipation source terms available in operational models like SWAN and WAVEWATCH III that will not be included in this section. For the purposes of this dissertation, only the most commonly used dissipation source terms will be included, which are whitecapping, bottom friction, and depth-induced breaking:

$$S_{diss} = S_{wc} + S_{bf} + S_{br}. \quad (51)$$

### A.3.1. *Whitcapping* $S_{wc}$

The term for whitcapping used in many wind wave models was first developed by Hasselmann in 1974 [24]. The default source term for whitcapping used in SWAN is based on the theory of Hasselmann and is taken from Komen et. al. 1984 and WAMDI in 1988 [35, 18]. The form is:

$$S_{wc} = -\Gamma \tilde{\sigma} \frac{k}{\tilde{k}} E(x, y, \sigma, \theta, t). \quad (52)$$

In this case:

$$\Gamma = C_{ds} \left( (1 - \delta) + \delta \frac{k}{\tilde{k}} \right) \left( \frac{\tilde{\sigma}}{\tilde{\sigma}_{PM}} \right)^p. \quad (53)$$

Here  $\tilde{\sigma}$  represents wave steepness and is defined as  $\tilde{\sigma} = \tilde{k} \sqrt{E_{tot}}$  and  $\tilde{\sigma}_{PM}$  is just  $\tilde{\sigma}$  of the Pierson-Moskowitz spectrum that is by default  $\tilde{\sigma}_{PM} = \sqrt{3.02 \times 10^{-3}}$ .  $C_{ds}$ ,  $n$ , and  $p$  are empirically tuned coefficients while  $\tilde{\sigma}$  and  $\tilde{k}$  are the mean frequency and wavenumbers defined in [18]:

$$E_{tot}(x, y) = \int_{\theta} \int_{\sigma} E(x, y, \sigma, \theta) d\theta d\sigma, \quad (54)$$

$$\tilde{\sigma}(x, y) = [E_{tot}^{-1} \int_{\theta} \int_{\sigma} \sigma^{-1} E(x, y, \sigma, \theta) d\theta d\sigma]^{-1}, \quad (55)$$

$$\tilde{k}(x, y) = [E_{tot}^{-1} \int_{\theta} \int_{\sigma} k^{-1/2} E(x, y, \sigma, \theta) d\theta d\sigma]^{-2}. \quad (56)$$

$C_{ds}$  by default is set to  $2.36e - 5$ ,  $p$  is set to 2,  $\delta$  is 1.

For the ST6 source term package, the whitcapping term is defined in the following way:

$$S_{wc}(x, y, f, \theta) = \begin{cases} 0, & \text{if } E(x, y, f, \theta) < E_T(x, y, f, \theta) \\ T_1(x, y, f, \theta) + T_2(x, y, f, \theta) & \text{if } E(x, y, f, \theta) \geq E_T(x, y, f, \theta), \end{cases} \quad (57)$$

Where the threshold spectral density,  $E_T$ , is defined as:

$$E_T(x, y, f, \theta) = \frac{2\pi B_{nt}}{A(x, y, f) c_g k^3}, \quad (58)$$

with  $B_{nt}$  is a constant  $1.225e - 3$  and  $A(x, y, f)$  as in (22). The two contributions of whitcapping are defined as follows:

$$T_1(x, y, f, \theta) = a_1 A(x, y, f) f \left[ \frac{\Delta(x, y, f)}{E(x, y, f)} \right]^L E(x, y, f, \theta), \quad (59)$$

$$T_2(x, y, f, \theta) = a_2 \left[ \int_{f_{low}}^f \left[ \frac{\Delta(x, y, f')}{E(x, y, f')} \right]^M df' \right] E(x, y, f, \theta).$$

Constants  $a_1$ ,  $a_2$ ,  $L$ ,  $M$  are calibrated based on empirical data and the function  $\Delta = E - E_T$  is the difference between variance density,  $E$ , and threshold variance density,  $E_T$ .

### A.3.2. *Bottom Friction* $S_{bf}$

Dissipation due to bottom friction plays an important role in shallow regions. There are many different formulations used in wind wave models, including the drag law theories and eddy-viscosity models [28]. The default implementation in SWAN is from the theory of Hasselmann in 1973 [23, 34]. The bottom friction term is defined as:

$$S_{bf}(x, y, \sigma, \theta, t) = -C_b \frac{\sigma^2}{\sinh^2(kd)} E(x, y, \sigma, \theta, t). \quad (60)$$

$C_b$  is a proportionality constant determined empirically and by default set to 0.038. It can be seen from the definition that the bottom friction becomes more relevant at lower wavenumber magnitude  $k$  and lower water depth  $d$ .

### A.3.3. Depth-Induced Breaking $S_{br}$

Lastly we have the source term due to depth induced breaking, also known as surf-zone breaking. The most widely used form of  $S_{br}$  is derived from the theories of Battjes and Janssen in 1978 [4]. Their theory approximates the energy lost due to breaking in shallow water as a bore. The theory was extended by Eldeberky and Battjes in 1995 to include multi-directional spectra [16] and takes the following form:

$$S_{br} = -\frac{\alpha_{bj} Q_b(x, y) \tilde{\sigma}(x, y)}{\beta^2(x, y) \pi} E(x, y, \sigma, \theta, t). \quad (61)$$

$\alpha_{bj}$  is a constant that is default set to 1,  $Q_b$  is the fraction of breaking waves,  $\tilde{\sigma}$  is the mean relative radian frequency, and  $\beta = \frac{H_{rms}}{H_{max}}$  is a parameter that varies over geographic space.  $Q_b$  is defined as:

$$Q_b = \begin{cases} 0 & \beta \leq 0.2 \\ Q_0 - \beta^2 \frac{Q_0 - e^{-\frac{Q_0 - 1}{\beta^2}}}{\beta^2 - e^{-\frac{Q_0 - 1}{\beta^2}}} & 0.2 \leq \beta \leq 1 \\ 1 & \beta > 1. \end{cases} \quad (62)$$

$Q_0$  in this case is calculated as:

$$Q_0 = \begin{cases} 0 & \beta \leq 0.5 \\ (2\beta - 1)^2 & 0.5 < \beta \leq 1. \end{cases} \quad (63)$$

The max expected wave height,  $H_{max}$  is defined as a constant times depth,  $H_{max} = \gamma d$ . By default,  $\gamma = 0.73$ . The root mean square wave height is calculated as  $H_{rms} = \sqrt{8m_0}$  with  $m_0$  being the zeroth moment as in (36). Lastly, the mean relative radian frequency is calculated as:

$$\tilde{\sigma}(x, y) = \frac{1}{E_{tot}} \int_{\sigma} \int_{\theta} \sigma E(x, y, \sigma, \theta) d\theta d\sigma. \quad (64)$$

## A.4. Summary of $S_{nl}$

Nonlinear interactions as represented by  $S_{nl}$  are conservative, in the sense that  $S_{nl}$  is always of zero average. This source term is responsible for redistributing action density amongst the spectrum due to wave wave interactions. The interactions can be thought of as energy exchanged due to resonance amongst wave components or if the waves are thought of as particles, collisions and exchange of momentum between each particle. The source term due to nonlinear interactions is usually split into a sum of two terms, nonlinear four wave interactions  $S_{nl4}$  and nonlinear three wave interactions  $S_{nl3}$ , also known as quadruplet wave interactions and triad wave interactions respectively.

### A.4.1. Quadruplets $S_{nl4}$

Four wave interactions can be thought of as when two pairs of harmonic waves resonate:

$$\begin{aligned} \sigma_1 + \sigma_2 &= \sigma_3 + \sigma_4, \\ \mathbf{k}_1 + \mathbf{k}_2 &= \mathbf{k}_3 + \mathbf{k}_4. \end{aligned} \quad (65)$$

This results in an exchange in energy between the four harmonic waves. Similarly, three wave interactions occur when a pair of harmonic waves resonate with a single harmonic wave. Due to the dispersion relation, it can be shown that the resonance conditions for triads can only occur in shallow water if Airy Wave Theory is assumed to hold true.

The theory describing the physics in the nonlinear four wave interactions was originally developed by Hasselmann [21, 22]. A similar form for the four-wave interactions was also found independently a couple of years later by Zakharov using the kinetic equation [65]. In the derivation by Hasselmann, the form of the quadruplet wave interactions was derived starting with an assumption of Airy Wave Theory and then conducting a perturbation analysis. This leads to the energy transfer amongst the spectrum to take a form of a Boltzmann integral that is of the form:

$$S_{nl4}(\mathbf{k}_4) = \iiint T_1(\mathbf{k}_1, \mathbf{k}_2, \mathbf{k}_1 + \mathbf{k}_2 - \mathbf{k}_4) E(\mathbf{k}_1) E(\mathbf{k}_2) E(\mathbf{k}_1 + \mathbf{k}_2 - \mathbf{k}_4) d\mathbf{k}_1 d\mathbf{k}_2 - \\ E(\mathbf{k}_4) \iiint T_2(\mathbf{k}_1, \mathbf{k}_2, \mathbf{k}_4) E(\mathbf{k}_1) E(\mathbf{k}_2) d\mathbf{k}_1 d\mathbf{k}_2. \quad (66)$$

The functions  $T_1$  and  $T_2$  are known as transfer coefficients that represent the amount of energy exchanging between each of the wavenumbers [28]. The first integral represents the passive part of the interaction with respect to wavenumber  $\mathbf{k}_4$  because it doesn't depend directly on  $E(\mathbf{k}_4)$ . The second integral represents the active part of the interaction, that is it does depend on  $E(\mathbf{k}_4)$  and it represents the amount of energy wavenumber  $\mathbf{k}_4$  is giving to the rest of the wavenumbers. In practice, the functions  $T_1$  and  $T_2$  are difficult to compute and more importantly, the Boltzmann integral form is extremely expensive computationally. There are some implementations that approximate the full Boltzmann integrals such as the Webb-Resio-Tracy (WRT) method [58]. However, calculating the full Boltzmann integrals are prohibitively expensive and thus limits wave models to simple test cases. For operational settings, a significant reduction in computation is necessary to implement the four wave interactions. A popular method to reduce the cost of computing  $S_{nl4}$  is called the discrete interaction approximation (DIA) [25][26]. The DIA simplifies the full Boltzmann integral by only considering resonance conditions in only two quadruplets. That is to say, instead of considering all possible four wave resonance conditions as in (65), the following reduced set is considered:

$$\begin{aligned}\sigma_1 &= \sigma_2 = \sigma, \\ \sigma_3 &= \sigma(1 + \lambda), \\ \sigma_4 &= \sigma(1 - \lambda).\end{aligned}\tag{67}$$

Here  $\lambda$  is an empirically determined constant that is  $\lambda = 0.25$ . Additionally, if the spectrum is in terms of relative radian frequency and direction  $(\sigma, \theta)$  the resonance conditions are restricted to the following two sets of angles: first (\*)  $\theta_1 = \theta_2 = \theta$ ,  $\theta_3 = \theta - 11.48^\circ$ ,  $\theta_4 = \theta + 33.56^\circ$ , and then second (\*\*)  $\theta_1 = \theta_2 = \theta$ ,  $\theta_3 = \theta + 11.48^\circ$ ,  $\theta_4 = \theta - 33.56^\circ$ . The source term  $S_{nl4}$  as prescribed by the DIA can then be defined as a sum of the contributions from the first set quadruplet angles (\*) and the second (\*\*):

$$S_{nl4}(\sigma, \theta) = S_{nl4}^*(\sigma, \theta) + S_{nl4}^{**}(\sigma, \theta).\tag{68}$$

Each contribution is then defined itself as a sum of approximations to the Boltzmann integrals:

$$S_{nl4}^*(\sigma, \theta) = 2\delta S_{nl4}(\alpha_1\sigma, \theta) - \delta S_{nl4}(\alpha_2\sigma, \theta) - \delta S_{nl4}(\alpha_3\sigma, \theta).\tag{69}$$

Where  $\alpha_1 = 1$ ,  $\alpha_2 = 1 + \lambda$ ,  $\alpha_3 = 1 - \lambda$ . Each contributor  $\delta S_{nl4}$  is defined for  $i = 1, 2, 3$ :

$$\begin{aligned}\delta S_{nl4}(\alpha_i\sigma, \theta) &= C \left( \frac{\sigma}{2\pi} \right)^{11} \left( E^2(\alpha_i\sigma, \theta) \left[ \frac{E(\alpha_i\sigma_3, \theta_3)}{(1 + \lambda)^4} + \frac{E(\alpha_i\sigma_4, \theta_4)}{(1 - \lambda)^4} \right] \right. \\ &\quad \left. - 2 \frac{E(\alpha_i\sigma, \theta)E(\alpha_i\sigma_3, \theta_3)E(\alpha_i\sigma_4, \theta_4)}{(1 - \lambda^2)^4} \right).\end{aligned}\tag{70}$$

$C$  is an empirically tuned constant. Note that  $S_{nl4}^{**}(\sigma, \theta)$  is the exact same as (69) but using the second set of angles (\*\*). From (70), we can see this source term is indeed nonlinear and in fact cubic with respect to the spectrum  $E(\sigma, \theta)$  at a given location. The DIA as shown above, or a variation of it, is used in the operational wind wave models SWAN, WAM, Mike21 and WAVEWATCH III. It is important to also note that there are other approximations to four-wave interactions than just the DIA and that this is a still active area of research. Some alternatives to the DIA include the two scale approximation (TSA), the RIAM method, and the Generalized Multiple DIA (MDIA) [48, 33, 56].

#### A.4.2. Triads $S_{nl3}$

Three wave interactions (or triads) are similar to four wave interactions, except as opposed to four wave interactions that occur in deep or shallow water, triads are typically segregated to shallow water [63]. This is because the resonance conditions for triads can not be met assuming the dispersion relation holds in deep water. The resonance conditions for three wave interactions are:

$$\begin{aligned}\sigma_1 \pm \sigma_2 &= \sigma_3, \\ \mathbf{k}_1 \pm \mathbf{k}_2 &= \mathbf{k}_3.\end{aligned}\tag{71}$$

Theoretical modelling of three wave interactions in the literature are often based on the Boussinesq type equations [28]. The Boussinesq type model is phase-resolving, which means on a large domain it is computationally expensive, highly

nonlinear, and the triad wave interactions occur implicitly within them. To include the effects of three wave interactions into the spectral wind wave model, significant simplifications are needed. A common approach in modern wind wave models is the lumped-triad approximation (LTA) of Eldeberky [15] and is of the following form:

$$S_{nl3}(\sigma, \theta) = S_{nl3}^+(\sigma, \theta) + S_{nl3}^-(\sigma, \theta). \quad (72)$$

The first term on the right hand side being:

$$S_{nl3}^+(\sigma, \theta) = \max [0, \alpha_{EB} 2\pi c c_g J^2 |\sin(\beta)| E^2(\sigma/2, \theta) - 2E(\sigma/2, \theta)E(\sigma, \theta)]. \quad (73)$$

$\alpha_{EB}$  is an empirically tuned coefficient,  $c$  is the phase speed (determined by the dispersion relation),  $c_g$  is the group velocity as defined in (10),  $J$  is called the interaction coefficient and is a function of water depth, phase speed, and wavenumber, and  $\beta$  is called the biphas. The second term on the right hand side is defined as:

$$S_{nl3}^-(\sigma, \theta) = -2S_{nl3}^+(2\sigma, \theta). \quad (74)$$

The original derivation can be found in [15], a more accessible summary can be found in [28]. The LTA is implemented in operational wind wave models SWAN, WAVEWATCH III and Mike21.

## CRediT authorship contribution statement

**Mark Loveland:** Methodology, Software, Validation, Writing - Original Draft. **Jessica Meixner:** Methodology, Writing - Review & Editing. **Eirik Valseeth:** Methodology, Writing - Review & Editing. **Clint Dawson:** Resources, Supervision, Project administration.

## References

- [1] Alves, J.H., Ardhuin, F., Babanin, A., Banner, M., Belibassakis, K., Benoit, M., Donelan, M., Groeneweg, J., Herbers, T., Hwang, P., Janssen, P., Janssen, T., Lavrenov, I., Magne, R., Monbaliu, J., Onorato, M., Polnikov, V., Resio, D., Rogers, W., Cavaleri, L., 2007. Wave modelling - the state of the art. *Progress In Oceanography* 75, 603–674. doi:10.1016/j.pcean.2007.05.005.
- [2] Ardag, D., Resio, D.T., 2019. Inconsistent spectral evolution in operational wave models due to inaccurate specification of nonlinear interactions. *Journal of Physical Oceanography* 49, 705 – 722. URL: <https://journals.ametsoc.org/view/journals/phoc/49/3/jpo-d-17-0162.1.xml>, doi:10.1175/JPO-D-17-0162.1.
- [3] Ardhuin, F., Rogers, E., Babanin, A.V., Filipot, J.F., Magne, R., Roland, A., van der Westhuysen, A., Queffeuilou, P., Lefevre, J.M., Aouf, L., Collard, F., 2010. Semiempirical dissipation source functions for ocean waves. part i: Definition, calibration, and validation. *Journal of Physical Oceanography* 40, 1917 – 1941. URL: <https://journals.ametsoc.org/view/journals/phoc/40/9/2010jpo4324.1.xml>, doi:10.1175/2010JPO4324.1.
- [4] Battjes, J.A., Janssen, J., 1978. Energy loss and set-up due to breaking of random waves, in: *Coastal engineering 1978*, pp. 569–587.
- [5] Beven II, J., Hagen, A., Berg, R., 2021. National hurricane center tropical cyclone report: Hurricane ida AL092021. URL: [https://www.nhc.noaa.gov/data/tcr/AL092021\\_Ida.pdf](https://www.nhc.noaa.gov/data/tcr/AL092021_Ida.pdf).
- [6] Booij, N., Ris, R.C., Holthuijsen, L.H., 1999. A third-generation wave model for coastal regions: 1. Model description and validation. *Journal of Geophysical Research: Oceans* 104, 7649–7666. URL: <https://agupubs.onlinelibrary.wiley.com/doi/abs/10.1029/98JC02622>, doi:https://doi.org/10.1029/98JC02622, arXiv:https://agupubs.onlinelibrary.wiley.com/doi/pdf/10.1029/98JC02622.
- [7] Boyd, S.C., Weaver, R.J., 2021. Replacing a third-generation wave model with a fetch based parametric solver in coastal estuaries. *Estuarine, Coastal and Shelf Science* 251, 107192. URL: <https://www.sciencedirect.com/science/article/pii/S0272771421000287>, doi:https://doi.org/10.1016/j.ecss.2021.107192.
- [8] Bunya, S., Dietrich, J.C., Westerink, J.J., Ebersole, B.A., Smith, J.M., Atkinson, J.H., Jensen, R., Resio, D.T., Luettich, R.A., Dawson, C., Cardone, V.J., Cox, A.T., Powell, M.D., Westerink, H.J., Roberts, H.J., 2010. A high-resolution coupled riverine flow, tide, wind, wind wave, and storm surge model for southern louisiana and mississippi. part i: Model development and validation. *Monthly Weather Review* 138, 345 – 377. URL: <https://journals.ametsoc.org/view/journals/mwre/138/2/2009mwr2906.1.xml>, doi:https://doi.org/10.1175/2009MWR2906.1.
- [9] US Department of Commerce, N., 2017. Hurricane Ike - September 2008. URL: [https://www.weather.gov/hgx/projects\\_ike08](https://www.weather.gov/hgx/projects_ike08).
- [10] Dietrich, J., Zijlema, M., Westerink, J., Holthuijsen, L., Dawson, C., Luettich, R., Jensen, R., Smith, J., Stelling, G., Stone, G., 2011. Modeling hurricane waves and storm surge using integrally-coupled, scalable computations. *Coastal Engineering* 58, 45–65. URL: <https://www.sciencedirect.com/science/article/pii/S0378383910001250>, doi:https://doi.org/10.1016/j.coastaleng.2010.08.001.
- [11] Dietrich, J.C., Bunya, S., Westerink, J.J., Ebersole, B.A., Smith, J.M., Atkinson, J.H., Jensen, R., Resio, D.T., Luettich, R.A., Dawson, C., Cardone, V.J., Cox, A.T., Powell, M.D., Westerink, H.J., Roberts, H.J., 2010. A high-resolution coupled riverine flow, tide, wind, wind wave, and storm surge model for southern louisiana and mississippi. part ii: Synoptic description and analysis of hurricanes katrina and rita. *Monthly Weather Review* 138, 378 – 404. URL: <https://journals.ametsoc.org/view/journals/mwre/138/2/2009mwr2907.1.xml>, doi:https://doi.org/10.1175/2009MWR2907.1.

- [12] Dietrich, J.C., Tanaka, S., Westerink, J.J., Dawson, C.N., Luettich, R., Zijlema, M., Holthuijsen, L.H., Smith, J., Westerink, L., Westerink, H., 2012. Performance of the unstructured-mesh, SWAN+ ADCIRC model in computing hurricane waves and surge. *Journal of Scientific Computing* 52, 468–497.
- [13] Donea, J., Quartapelle, L., 1992. An introduction to finite element methods for transient advection problems. *Computer Methods in Applied Mechanics and Engineering* 95, 169–203. URL: <https://www.sciencedirect.com/science/article/pii/004578259290139B>, doi:[https://doi.org/10.1016/0045-7825\(92\)90139-B](https://doi.org/10.1016/0045-7825(92)90139-B).
- [14] Egbert, G.D., Erofeeva, S.Y., 2002. Efficient Inverse Modeling of Barotropic Ocean Tides. *Journal of Atmospheric and Oceanic Technology* 19, 183 – 204. URL: [https://journals.ametsoc.org/view/journals/atot/19/2/1520-0426\\_2002\\_019\\_0183\\_eimobo\\_2\\_0\\_co\\_2.xml](https://journals.ametsoc.org/view/journals/atot/19/2/1520-0426_2002_019_0183_eimobo_2_0_co_2.xml), doi:10.1175/1520-0426(2002)019<0183:EIMOBO>2.0.CO;2.
- [15] Eldeberky, Y., 1997. Nonlinear transformation of wave spectra in the nearshore zone. *Oceanographic Literature Review* 4, 297.
- [16] Eldeberky, Y., Battjes, J.A., 1996. Spectral modeling of wave breaking: Application to Boussinesq equations. *Journal of Geophysical Research: Oceans* 101, 1253–1264. URL: <https://agupubs.onlinelibrary.wiley.com/doi/abs/10.1029/95JC03219>, doi:<https://doi.org/10.1029/95JC03219>, arXiv:<https://agupubs.onlinelibrary.wiley.com/doi/pdf/10.1029/95JC03219>.
- [17] Fleming, J.G., Fulcher, C.W., Luettich, R.A., Estrade, B.D., Allen, G.D., Winer, H.S., 2008. A real time storm surge forecasting system using ADCIRC, in: *Estuarine and coastal modeling* (2007), pp. 893–912.
- [18] Group, T.W., 1988. The WAM model—a third generation ocean wave prediction model. *Journal of Physical Oceanography* 18, 1775–1810.
- [19] Hanchey, A., Schnall, A., Bayleyegn, T., Jiva, S., Khan, A., Siegel, V., Funk, R., Svendsen, E., 2021. Notes from the field: Deaths related to hurricane ida reported by media—nine states, august 29–september 9, 2021. *Morbidity and Mortality Weekly Report* 70, 1385.
- [20] Hasselmann, D.E., Dunkel, M., Ewing, J.A., 01 Aug. 1980. Directional Wave Spectra Observed during JONSWAP 1973. *Journal of Physical Oceanography* 10, 1264 – 1280. URL: [https://journals.ametsoc.org/view/journals/phoc/10/8/1520-0485\\_1980\\_010\\_1264\\_dwsodj\\_2\\_0\\_co\\_2.xml](https://journals.ametsoc.org/view/journals/phoc/10/8/1520-0485_1980_010_1264_dwsodj_2_0_co_2.xml), doi:10.1175/1520-0485(1980)010<1264:DWSODJ>2.0.CO;2.
- [21] Hasselmann, K., 1962. On the non-linear energy transfer in a gravity-wave spectrum part I. general theory. *Journal of Fluid Mechanics* 12, 481–500. doi:10.1017/S0022112062000373.
- [22] Hasselmann, K., 1968. Weak-interaction theory of ocean waves, in: *Basic developments in fluid dynamics*. Academic Press, pp. 117–182.
- [23] Hasselmann, K., Barnett, T., Bouws, E., Carlson, H., Cartwright, D., Enke, K., Ewing, J., Gienapp, H., Hasselmann, D., Kruseman, P., Meerburg, A., Muller, P., Olbers, D., Richter, K., Sell, W., Walden, H., 1973. Measurements of wind-wave growth and swell decay during the Joint North Sea Wave Project (JONSWAP). *Deut. Hydrogr. Z.* 8, 1–95.
- [24] Hasselmann, K.F., 1974. On the spectral dissipation of ocean waves due to white capping. *Boundary-Layer Meteorology* 6, 107–127.
- [25] Hasselmann, S., Hasselmann, K., 01 Nov. 1985. Computations and parameterizations of the nonlinear energy transfer in a gravity-wave spectrum. part i: A new method for efficient computations of the exact nonlinear transfer integral. *Journal of Physical Oceanography* 15, 1369 – 1377. URL: [https://journals.ametsoc.org/view/journals/phoc/15/11/1520-0485\\_1985\\_015\\_1369\\_capotn\\_2\\_0\\_co\\_2.xml](https://journals.ametsoc.org/view/journals/phoc/15/11/1520-0485_1985_015_1369_capotn_2_0_co_2.xml), doi:10.1175/1520-0485(1985)015<1369:CAPOTN>2.0.CO;2.
- [26] Hasselmann, S., Hasselmann, K., Allender, J., Barnett, T., 1985. Computations and parameterizations of the nonlinear energy transfer in a gravity-wave spectrum. part ii: Parameterizations of the nonlinear energy transfer for application in wave models. *Journal of Physical Oceanography* 15, 1378–1391.
- [27] Holthuijsen, L., Boer, S., et al., 1988. *Wave forecasting for moving and stationary targets*. doi:10.1017/CB09780511618536.
- [28] Holthuijsen, L.H., 2007. *Waves in Oceanic and Coastal Waters*. Cambridge University Press. doi:10.1017/CB09780511618536.
- [29] Hope, M.E., Westerink, J.J., Kennedy, A.B., Kerr, P., Dietrich, J.C., Dawson, C., Bender, C.J., Smith, J., Jensen, R.E., Zijlema, M., et al., 2013. Hindcast and validation of Hurricane Ike (2008) waves, forerunner, and storm surge. *Journal of Geophysical Research: Oceans* 118, 4424–4460.
- [30] Janssen, P., 2008. Progress in ocean wave forecasting. *Journal of Computational Physics* 227, 3572–3594. doi:10.1016/j.jcp.2007.04.029.
- [31] Kennedy, A.B., Gravois, U., Zachry, B.C., Westerink, J.J., Hope, M.E., Dietrich, J.C., Powell, M.D., Cox, A.T., Luettich Jr., R.A., Dean, R.G., 2011. Origin of the Hurricane Ike forerunner surge. *Geophysical Research Letters* 38. URL: <https://agupubs.onlinelibrary.wiley.com/doi/abs/10.1029/2011GL047090>, doi:<https://doi.org/10.1029/2011GL047090>, arXiv:<https://agupubs.onlinelibrary.wiley.com/doi/pdf/10.1029/2011GL047090>.
- [32] Khandekar, M., 1989. *Operational Analysis and Prediction of Ocean Wind Waves*. volume 33. doi:10.1007/978-1-4613-8952-1.
- [33] Komatsu, K., Masuda, A., 1996. A new scheme of nonlinear energy transfer among wind waves: RIAM method-algorithm and performance. *Journal of Oceanography* 52, 509–537.
- [34] Komen, G.J., Cavaleri, L., Donelan, M., Hasselmann, K., Hasselmann, S., Janssen, P.A.E.M., 1994. *Dynamics and Modelling of Ocean Waves*. Cambridge University Press. doi:10.1017/CB09780511628955.
- [35] Komen, G.J., Hasselmann, S., Hasselmann, K., 1984. On the existence of a fully developed wind-sea spectrum. *Journal of Physical Oceanography* 14, 1271 – 1285. URL: [https://journals.ametsoc.org/view/journals/phoc/14/8/1520-0485\\_1984\\_014\\_1271\\_oteoaf\\_2\\_0\\_co\\_2.xml](https://journals.ametsoc.org/view/journals/phoc/14/8/1520-0485_1984_014_1271_oteoaf_2_0_co_2.xml), doi:10.1175/1520-0485(1984)014<1271:OTE0AF>2.0.CO;2.
- [36] Landsea, C., Franklin, J., Beven, J., 2015. *The revised atlantic hurricane database (hurdat2)*. NOAA/NHC.[Available online at [nhc.noaa.gov](http://nhc.noaa.gov)].
- [37] LeBlond, P., Mysak, L., 1981. *Waves in the Ocean*. ISSN, Elsevier Science. URL: [https://books.google.com/books?id=TYGIwzz\\_k8kC](https://books.google.com/books?id=TYGIwzz_k8kC).
- [38] LeVeque, R.J., Leveque, R.J., 1992. *Numerical methods for conservation laws*. volume 214. Springer.
- [39] Longuet-Higgins, M.S., Stewart, R.W., 1962. Radiation stress and mass transport in gravity waves, with application to ‘surf beats’. *Journal of Fluid Mechanics* 13, 481–504. doi:10.1017/S0022112062000877.
- [40] Luettich, R.A., Westerink, J.J., 2004. Formulation and numerical implementation of the 2D/3D ADCIRC finite element model version 44. *XX. volume 20*. R. Luettich Chapel Hill, NC, USA.

- [41] McAlpin, T.O., Letter, J.V., Bryant, M.A., Emiren, A.G., Brown, G.L., Savant, G., Wisemiller, B.W., Sulayman, J.A., Trahan, C.J., 2020. New York/New Jersey harbor sedimentation study: numerical modeling of hydrodynamics and sediment transport.
- [42] Meixner, J., 2013. Discontinuous Galerkin Methods for Spectral Wave/Circulation Modeling. Ph.D. thesis.
- [43] Miles, J.W., 1957. On the generation of surface waves by shear flows. *Journal of Fluid Mechanics* 3, 185–204. doi:10.1017/S0022112057000567.
- [44] Moghimi, S., Van der Westhuysen, A., Abdolali, A., Myers, E., Vinogradov, S., Ma, Z., Liu, F., Mehra, A., Kurkowski, N., 2020. Development of an esmf based flexible coupling application of adcirc and wavewatch iii for high fidelity coastal inundation studies. *Journal of Marine Science and Engineering* 8, 308.
- [45] Monbaliu, J., 2003. Chapter 5 Spectral wave models in coastal areas, in: Lakhan, V. (Ed.), *Advances in Coastal Modeling*. Elsevier. volume 67 of *Elsevier Oceanography Series*, pp. 133–158. URL: <https://www.sciencedirect.com/science/article/pii/S0422989403801228>, doi:[https://doi.org/10.1016/S0422-9894\(03\)80122-8](https://doi.org/10.1016/S0422-9894(03)80122-8).
- [46] Phillips, O.M., 1957. On the generation of waves by turbulent wind. *Journal of Fluid Mechanics* 2, 417–445. doi:10.1017/S0022112057000233.
- [47] Pironneau, O., Pironneau, O., 1989. *Finite element methods for fluids*. Wiley Chichester.
- [48] Resio, D.T., Perrie, W., 2008. A two-scale approximation for efficient representation of nonlinear energy transfers in a wind wave spectrum. part i: Theoretical development. *Journal of Physical Oceanography* 38, 2801 – 2816. URL: <https://journals.ametsoc.org/view/journals/phoc/38/12/2008jpo3713.1.xml>, doi:10.1175/2008JP03713.1.
- [49] Rogers, W.E., Babanin, A.V., Wang, D.W., 2012. Observation-consistent input and whitecapping dissipation in a model for wind-generated surface waves: Description and simple calculations. *Journal of Atmospheric and Oceanic Technology* 29, 1329 – 1346. URL: [https://journals.ametsoc.org/view/journals/atot/29/9/jtech-d-11-00092\\_1.xml](https://journals.ametsoc.org/view/journals/atot/29/9/jtech-d-11-00092_1.xml), doi:10.1175/JTECH-D-11-00092.1.
- [50] Roland, A., 2008. Development of WWM II: Spectral wave modeling on unstructured meshes. Ph.D. thesis.
- [51] Roland, A., 2012. Application of Residual Distribution (RD) schemes to the geographical part of the Wave Action Equation, in: ECMWF workshop on ocean waves, pp. 25–27.
- [52] Roland, A., Zhang, Y.J., Wang, H.V., Meng, Y., Teng, Y.C., Maderich, V., Brovchenko, I., Dutour-Sikiric, M., Zanke, U., 2012. A fully coupled 3d wave-current interaction model on unstructured grids. *Journal of Geophysical Research: Oceans* 117.
- [53] SWAMP, 1985. *Ocean Wave Modeling*. Springer. doi:10.1007/978-1-4757-6055-2.
- [54] Team, S., et al., 2022. SWAN, Scientific and Technical Documentation, SWAN Cycle III version 41.41. <http://www.swan.tudelft.nl>, Delft University of Technology URL: <https://swanmodel.sourceforge.io/download/zip/swantech.pdf>.
- [55] Tolman, H.L., 1991. A Third-Generation Model for Wind Waves on Slowly Varying, Unsteady, and Inhomogeneous Depths and Currents. *Journal of Physical Oceanography* 21, 782 – 797. URL: [https://journals.ametsoc.org/view/journals/phoc/21/6/1520-0485\\_1991\\_021\\_0782\\_atgmfw\\_2\\_0\\_co\\_2.xml](https://journals.ametsoc.org/view/journals/phoc/21/6/1520-0485_1991_021_0782_atgmfw_2_0_co_2.xml), doi:10.1175/1520-0485(1991)021<0782:ATGMFW>2.0.CO;2.
- [56] Tolman, H.L., 2013. A generalized multiple discrete interaction approximation for resonant four-wave interactions in wind wave models. *Ocean Modelling* 70, 11–24.
- [57] Tolman, H.L., Chalikov, D., 01 Nov. 1996. Source terms in a third-generation wind wave model. *Journal of Physical Oceanography* 26, 2497 – 2518. URL: [https://journals.ametsoc.org/view/journals/phoc/26/11/1520-0485\\_1996\\_026\\_2497\\_stiatg\\_2\\_0\\_co\\_2.xml](https://journals.ametsoc.org/view/journals/phoc/26/11/1520-0485_1996_026_2497_stiatg_2_0_co_2.xml), doi:10.1175/1520-0485(1996)026<2497:STIATG>2.0.CO;2.
- [58] Tracy, B.A., Resio, D.T., 1982. Theory and calculation of the nonlinear energy transfer between sea waves in deep water., in: *Proceedings of the Army Numerical and Computers Analysis Conference, US Army Research Office.* p. 457.
- [59] Umesh, P., Behera, M.R., 2020. Performance evaluation of input-dissipation parameterizations in wavewatch iii and comparison of wave hindcast with nested wavewatch iii-swam in the indian seas. *Ocean Engineering* 202, 106959.
- [60] Warren, I., Bach, H., 1992. Mike 21: a modelling system for estuaries, coastal waters and seas. *Environmental Software* 7, 229–240.
- [61] Westerink, J.J., Luettich, R.A., Feyen, J.C., Atkinson, J.H., Dawson, C., Roberts, H.J., Powell, M.D., Dunion, J.P., Kubatko, E.J., Pourtaheri, H., 2008. A basin-to channel-scale unstructured grid hurricane storm surge model applied to southern Louisiana. *Monthly weather review* 136, 833–864.
- [62] Wu, J., 1982. Wind-stress coefficients over sea surface from breeze to hurricane. *Journal of Geophysical Research: Oceans* 87, 9704–9706. URL: <https://agupubs.onlinelibrary.wiley.com/doi/abs/10.1029/JC087iC12p09704>, doi:<https://doi.org/10.1029/JC087iC12p09704>, arXiv:<https://agupubs.onlinelibrary.wiley.com/doi/pdf/10.1029/JC087iC12p09704>.
- [63] Young, I.R., 1999. *Wind generated ocean waves*. Elsevier.
- [64] Yurovskaya, M., Kudryavtsev, V., Chapron, B., 2023. A self-similar description of the wave fields generated by tropical cyclones. *Ocean Modelling* 183, 102184. URL: <https://www.sciencedirect.com/science/article/pii/S1463500323000252>, doi:<https://doi.org/10.1016/j.ocemod.2023.102184>.
- [65] Zakharov, V.E., 1968. Stability of periodic waves of finite amplitude on the surface of a deep fluid. *Journal of Applied Mechanics and Technical Physics* 9, 190–194.
- [66] Zane, D.F., Bayleyegn, T.M., Hellsten, J., Beal, R., Beasley, C., Haywood, T., Wiltz-Beckham, D., Wolkin, A.F., 2011. Tracking deaths related to hurricane Ike, Texas, 2008. *Disaster medicine and public health preparedness* 5, 23–28.